Linköping Studies in Science and Technology
Dissertation No. 2376

Venturing Further into the Field of 2D Materials and their Laminated Parent Phases

Pernilla Helmer

LINKÖPING UNIVERSITY

Linköping Studies in Science and Technology
Dissertation Thesis No. 2376

Venturing Further into the Field of 2D Materials and their Laminated Parent Phases

Pernilla Helmer

Materials Design Division
Department of Physics, Chemistry and Biology (IFM)
Linköping University, SE-581 83, Linköping, Sweden

Decorating the cover is a unicorn of atoms, kindly prompted by Adam Carlsson in the image generator DALL-E 3. Thank you, Adam.

Printed by LiU-Tryck, Linköping, Sweden 2024

ISBN: 978-91-8075-543-6 (tryckt)
ISBN 978-91-8075-544-3 (pdf)
DOI: doi.org/10.3384/9789180755443
ISSN: 0345-7524

Till Arne, Roland och Claudio

Abstract

The field of 2D materials is a relatively young and rapidly growing area within materials science, which is concerned with atomically thin states of matter. Because of their intrinsic 2D morphology, 2D materials have exceptionally high surface to weight or surface to volume ratio. This renders them excellent candidates for surface-sensitive applications such as catalysis and energy storage, which can aid us in the transition to a more sustainable society. 2D materials are also interesting because they show properties intrinsically different from those of their 3D counterparts, expanding the attainable property space within materials science. A 2D material can be synthesised by either a bottom-up or top-down approach. The focus here is on the latter, where the 2D material is derived by either mechanical exfoliation or selective etching of a 3D nanolaminated parent phase.

A 3D laminate can typically be assigned to one of two types, depending on the type of interlayer bonding: van der Waals (vdW) or chemical bonding. In a vdW bonded phase, the constituent layers are kept together into their 3D form by rather weak vdW forces, while in the latter type, the layers are bound more strongly by chemical interactions (i.e., covalent, ionic and metallic bonds). The first 2D materials were derived from vdW-phases, which can be exfoliated by mechanical methods. In a chemically bound laminated phase, the inter layer bonding is stronger, and more complex methods are required for exfoliation of these phases into 2D. This thesis concerns the computational study and development of novel 2D materials through exploration of 3D nanolaminated structures, assessment of their phase stability, and potential for conversion into 2D. The 2D derivatives are in turn studied through prediction of dynamical stability, termination configuration, and evaluation of electronic properties.

Paper III and IV each addresses a family of van der Waals structures. The family of 3D materials studied in Paper III was chosen because it was recently demonstrated as possible to use for derivation of so called 2D MXenes, while the 2D form of $NbOCl_2$, from the family studied in Paper IV, has been shown to exhibit exciting optical properties. Both projects focus on identification of parent 3D materials, their exfoliation from 3D to

2D, and the electronic properties of the studied phases. In each project, a range of different chemical compositions is considered, chosen based on the experimentally known members of the respective families. A 3D structural ground state is predicted for each composition and prototype, and the dynamical stability with respect to lattice vibrations is established for each identified structure. To assure the experimental relevance of each considered 3D phase, the thermodynamical stability of each structure is assessed via the formation enthalpy with respect to competing phases, identifying seven stable structures in Paper III, and 17 in Paper IV, all of which are also found dynamically stable. Evaluation of the exfoliation energy for all these phases indicates that 3D to 2D conversion is possible. The electronic band structure and density of states were evaluated both for the 2D materials – being the primary focus in both projects – and their 3D parent phases. Although the bandgap for semiconducting phases is generally increased upon exfoliation, the electronic properties are mostly retained when exfoliating the vdW phases studied in this thesis.

Paper I, II and V address chemically bonded 3D phases and their 2D derivatives. In these 3D phases, auxiliary atoms are interleaved between the 2D units, which needs to be selectively etched to form the corresponding 2D material. Additionally, new terminating species – so called terminations – may attach to the surfaces of the 2D units exposed during etching. Paper I presents an analysis of bonding characteristics in a group of nanolaminated 3D chemically bonded borides: Mo_2SiB_2, Ti_4MoSiB_2, and Ti_5SiB_2, out of which only the two former are observed experimentally. We identify a peak of antibonding states at the Fermi level for Ti_5SiB_2 as a reason why full elemental substitution of Mo is not achieved experimentally. Papers II and V instead focus on 2D materials derived from chemical 3D parent phases. They go beyond the 2D transition metal carbides and nitrides (MXenes), which until recently were the only 2D materials synthesised through selective etching. Paper II is a study of possible termination configurations on the first 2D boride $Mo_{4/3}B_{2-x}T_z$ – boridene – which is identified as being a conductor or small bandgap semiconductor, depending on the terminating species and specific configuration.

In Paper V, a computational methodology for simulation of the selective etching process is employed to predict the possibility of etching Y from YM_2X_2, where the transition metal M and metalloid or nonmetal X are chosen to cover a large compositional space. This results in the prediction of 15 stable 2D structures, out of which nine are not previously investigated. All 2D structures are found to be either metallic or semimetallic.

In this thesis, several different computational tools are used to predict and study laminated 3D phases and their corresponding 2D derivatives, assessing their properties considering both purely hypothetical and experimentally realised structures. Experimental relevance is central to all calcu-

lations, either by complementing already established experimental results, or by rigorous assessment of thermodynamical and dynamical stability to estimate the potential for experimental synthesis. The thesis expands our knowledge of 3D laminated phases and their 2D derivatives, and identifies several new phases which are likely possible to synthesise.

Populärvetenskaplig Sammanfattning

Det moderna samhället står idag inför en oerhörd utmaning, där den ökande globala genomsnittstemperaturen – ett resultat av vår omfattande förbränning av fossila bränslen – orsakar svåröverskådliga och långtgående allvarliga konsekvenser i stora delar av världen. Samtidigt ökar efterfrågan på billig energi allt eftersom vi blir fler människor på jorden, och varje individ kräver allt mer resurser för att möta allt högre förväntningar på levnadsstandard. Det är kort och gott inte en enkel ekvation att lösa. Denna avhandling relaterar specifikt, om än indirekt, till hur energi kan utvinnas och lagras mer effektivt än idag, vilket är en oerhört viktig pusselbit för ett mer hållbart framtida samhälle.

Det finns många olika sätt att lagra energi, till exempel mekanisk, kemisk och elektrokemisk lagring. Olika bränslen, inklusive fossila bränslen, är exempel på kemisk energilagring. Kemisk energi utvinns ur bränslet genom att bränslemolekylerna deltar i en kemisk process, där skapandet av nya kemiska bindningar frigör energi. I de flesta fall är koldioxid en av slutprodukterna vid utvinning av kemisk energi, även när det kommer till förnyelsebara bränslen som etanol och förnyelsebar metangas. Därför är utvinning av kemisk energi sällan problemfri även om den inte sker ur fossila bränslen. Ett sätt att lagra kemisk energi utan dessa problem är att lagra den i form av vätgas, som vid förbränning har vatten som slutprodukt. Att framställa vätgas är dock energikrävande och effektiva katalysatorer behövs för att det ska kunna konkurrera med andra bränslen. Den mest effektiva katalysatorn vi har idag är platina – en ädelmetall som är dyrare än guld.

Batterier används för elektrokemisk energilagring, genom att lagra laddning i form av joner som kan utvinnas som elektrisk energi. Det finns flera olika sätt att konstruera den kemiska sammansättningen för ett batteri, som alla har sina för- och nackdelar. Ett klassiskt bilbatteri har till exempel en helt annan kemi och andra egenskaper än ett uppladdningsbart batteri för en elcykel. Inom kommersiell batteritillverkning förekommer dock bara ett fåtal kemier som är tillräckligt säkra och kostnadseffektiva,

och den drastiskt ökande efterfrågan på batterier gör att det därför blir hög konkurrens om råvaror. Det finns således ett stort behov både av att utveckla nya kemier för batterier, och av att utveckla effektivare sätt att utnyttja råvarorna vi redan använder.

Tvådimensionella (2D) material är en relativt ung gren inom materialforskningsområdet, med en närmst oändlig uppsjö av potentiella tillämpningsområden. Ett 2D-material är bara ett till några få atomlager tjockt, och är således så tunt ett material över huvud taget kan bli. Detta medför att 2D-material har en väldigt stor yta i förhållande till volym och antal atomer, vilket gör dem till utmärkta kandidater för diverse tillämpningar där ett materials yta är dess viktigaste egenskap. Bland annat är de potentiella kandidater både som katalysatorer för flera olika reaktioner, och för jonlagring i batterier.

Denna avhandling är fokuserad på utveckling av nya 2D-material samt karakterisering av dessa utifrån olika aspekter. Det finns olika metoder för att framställa 2D-material, men de flesta har gemensamt att de utgår från ett 3D-material där atomerna redan ligger i ordnade lager och sedan på olika sätt separerar dessa lager från varandra för att framställa motsvarande 2D-material. Den forskning som presenteras i denna avhandling är därför inte begränsad till bara 2D-material, utan studerar även lagrade 3D-material som skulle kunna användas för framställning av nya 2D-material. I artikel I studeras därför en grupp lagrade 3D-material, med målet att förstå varför vissa av dem går att framställa experimentellt medan andra inte gör det. De övriga artiklarna undersöker i första hand 2D-material. I artikel II studeras de så kallade termineringarna – enskilda atomer eller väldigt små grupper av atomer som fäster på ytan av vissa typer av 2D-material och påverkar deras egenskaper – och hur dessa påverkar de elektroniska egenskaperna hos materialet. I artikel III, IV och V utgår respektive studie från en lagrad 3D-struktur där atomerna byts ut mot olika kemiska sammansättningar. 3D-material som är intressanta som utgångsmaterial för framställning av nya 2D-material identifieras genom olika typer av stabilitetsanalys, och de motsvarande 2D-materialen studeras i detalj, specifikt ur perspektivet av elektronegenskaper. Vi förutspår flera nya både 3D- och 2D-material, varav vissa är ledande, andra är halvledande, och några har mer exotiska egenskaper någonstans mittemellan.

Som tidigare nämnt så är resultatet av den forskning som ingår i denna avhandling främst relevant för att lösa klimatkrisen ur ett indirekt perspektiv; vi undersöker inte hur materialen presterar för batteriapplikationer, och endast ett material studeras för katalys. Dock måste varje meningsfull upptäckt börja någonstans, och detta kräver en gedigen och systematisk grundforskning, eftersom vi inte vill förlita oss på att slumpen låter oss hitta nästa banbrytande material. Denna avhandling är en del av just denna grundforskning, där nya, oupptäckta material förutspås och grundläggande

egenskaper för nyupptäckta material undersöks. Andra forskare, framförallt inom experimentella områden, har sedan möjlighet att bygga vidare på de resultat som presenteras här, och kanske leder våra upptäckter så småningom till att nya material med verkligt användbara egenskaper realiseras.

Preface

This thesis is the result of my PhD studies, conducted between March 2019 and April 2024 at the Thin Film Physics and the Materials Design divisions, department of Physics, Chemistry and Biology (IFM) at Linköping University. The work has been concluded under the main supervision of Prof. Johanna Rosén, and the co-supervision of Ass. Prof. Jonas Björk and Ass. Prof. Matin Dahlqvist. The thesis is a continuation of the Licentiate Thesis No. 1925 "*A Computational Venture into the Realm of Laminated Borides and their 2D Derivatives*", which was defended on the 4$^{\text{th}}$ of March 2022.

Financial support from the Swedish Research Council, VR (grant number 2019-05047 and 2022-06099), the Göran Gustavsson Foundation for Research in Natural Sciences and Medicine, and the Knut and Alice Wallenberg (KAW) foundation has made this work possible. Simulations has been carried out using resources provided by the National Academic Infrastructure for Supercomputing in Sweden (NAISS) and Swedish National Infrastructure for Computing (SNIC), using the NSC, PDC and HPC2N computer clusters.

Acknowledgements

The completion of this thesis has had its fair share of ups and downs, but here it is, finally, and I would like to express my sincerest gratitude to those who have made it possible.

First and foremost, I want to acknowledge the support of my supervisors, Johanna Rosén, Jonas Björk och Martin Dahlqvist. Thank you, Johanna, for giving me the opportunity of perusing a doctoral degree, and teaching me what it is to be a researcher. I thoroughly appreciate the enthusiasm you have shown for my results, in particular when I've felt them to be mediocre, and that you have always been available when needed, especially these last few weeks. I also want to thank you for letting me write the last manuscripts in LaTeX, I've never hated writing papers less. And to Jonas and Martin, of course, thank you for all the expertise you have generously shared with me, but also for the beers and fun times that you have shared maybe even more generously.

Next I would like to express my gratitude to Joseph Halim, or Joe, who took care of me and showed me around when I first arrived to Linköping. Thank you for being my friend, for showing me all the best places and for always being up for hanging out. Special thanks also to Marius Rodner, who included me into the IFM PhD community, to Luis Casillas and Johan Nyman who were around even during that terrible time of the corona pandemic and helped me stay somewhat sane, and to Kaifeng Niu and Adam Carlsson, who have been my much appreciated office mates and friends throughout this time. Thank you so much for being there and being you.

I would also like to show my appreciation for all the people whom I've been hanging out with at lunch, chatting with in the corridors and the coffee room, and without whom my time here would not have been the same. Thank you Claudia, Arnaud, Davide, Julia, Ania, Rodrigo, Guilherme, Lida, Rana, Lin, Anna, Gulzada, Amaia, Anton, Marcus, Marian, Thirza, Nikos, Sven, Sachin, Ingemar, Jens, Jie, Karina, Fredrik, Victor, Rafael, a different Nikos, Laurent, Andreas, and many more. Thank you to all the members of the Doctoral Student Council, as well as the different people around IFM who have helped us in our endeavours. In particular, thank you

Per Eklund, Stefan Klintström and Caroline Brommesson, for everything you do and have done for the IFM PhD students.

Thank you Björn Alling, Ferenc Tasnadi, and Peter Münger, for being such enthusiastic lecturers and teachers. And to Arne Holgersson, Roland Johansson and Claudio Verdozzi: without your inspiration I would be somewhere different today.

Finally, I would like to thank my family and friends for listening when I've needed someone to complain to as well as to be excited with. In particular, thank you Sebastian Pfaff and Tim Almqvist, for all the IT support, as well as other support, that you have given me throughout the years. And last but not least, thank you Elliot, for always being there for me.

List of Included Papers

Paper I: Investigation of Out-Of-Plane Ordered Ti_4MoSiB_2 from First Principles
Pernilla Helmer, Hans Lind, Martin Dahlqvist, and Johanna Rosen
Journal of Physics: Condensed Matter, 2022, **34**, 185501

Paper II: Investigation of 2D Boridene from First Principles and Experiments
Pernilla Helmer, Joseph Halim, Jie Zhou, Roopathy Mohan, Björn Wickman, Jonas Björk, and Johanna Rosen
Advanced Functional Materials, 2022, **32**, 2109060

Paper III: Computational Screening of Chalcogen-Terminated Multilayer MXenes and M_2AX Precursors
Pernilla Helmer, Jonas Björk, and Johanna Rosen
Submitted

Paper IV: Computational Screening of the MOX_2 Transition Metal Oxydihalides with M=V, Nb, Ta, Mo, Ru and Os, and X=Cl, Br, I
Pernilla Helmer, Martin Dahlqvist, and Johanna Rosen
In manuscript

Paper V: Expanding the Structural and Compositional Space of 2D $M_2X_2T_y$ Materials through Simulated Etching of 3D YM_2X_2 Parent Phases
Pernilla Helmer, Rodrigo Ronchi, Martin Dahlqvist, Jonas Björk, and Johanna Rosen
In manuscript

Contributions: In Papers II, III and IV, I was responsible for all calculations and related data analysis and presentation. In Paper I, I performed the calculations and data analysis related to the chemical bonding, and in Paper V I performed the thermodynamical stability screening, the evaluation of dynamical stability and electronic structure, and the related data analysis. I wrote the majority of all papers, made all the figures and gave constructive feedback on the sections written by my coauthors.

Related Papers

Single Crystal Growth and Structural Characterization of Theoretically Predicted Nanolaminates $M_2Al_2C_3$, Where M = Sc and Er
Quanzheng Tao, Pernilla Helmer, Laurent Jouffret, Martin Dahlqvist, Jun Lu, Jie Zhou, and Johanna Rosen
Crystal Growth and Design, 2020, **20**, 7640

Out-Of-Plane Ordered Laminate Borides and Their 2D Ti-Based Derivative from Chemical Exfoliation
Martin Dahlqvist, Jie Zhou, Ingemar Persson, Bilal Ahmed, Jun Lu, Joseph Halim, Quanzheng Tao, Justinas Palisaitis, Jimmy Thörnberg, Pernilla Helmer, Lars Hultman, Per O. Å. Persson, and Johanna Rosen
Advanced Materials, 2021, **33**, 2008361

Experimental and Theoretical Investigations of Out-of-Plane Ordered Nanolaminate Transition Metal Borides: M_4CrSiB_2 (M = Mo, W, Nb)
Joseph Halim, Pernilla Helmer, Justinas Palisaitis, Martin Dahlqvist, Jimmy Thörnberg, Per O. Å. Persson, and Johanna Rosen
Inorganic Chemistry, 2023, **62**, 5341–5347

Synthesis of Cr2AuC via Thermal Substitution Reaction in Au-Covered Cr2GaC and Cr2GeC Thin Films
Yuchen Shi, Shun Kashiwaya, Pernilla Helmer, Jun Lu, Mike Andersson, Andrejs Petruhins, Johanna Rosen, and Lars Hultman
Results in Materials, 2023 **18**, 100403

Contents

Chapter 1

Introduction to 2D materials

The search for, utilisation, and manipulation of materials is a central human activity, to the point where the periods of early human history are named by the characteristic material of that time. The utilisation of different materials to enhance our own capabilities is something that distinguishes us from other species, and it has let us become experts at performing a great variety of tasks without having to wait for evolution to equip us appropriately.

Different ways have over time been discovered to improve and tailor material properties to better suit our needs and desires. Alloying, for instance, was used during the bronze age to improve the properties of copper, by alloying with predominately tin or zinc to form bronze. This improves the hardness compared to pure copper and renders bronze a more useful material for making sharp or durable items. Yet other ways of manipulating a material is by heating, for instance the burning of clay to make ceramics, or by mixing chemicals to synthesise new materials, such as gunpowder. Indeed, considerable human activity throughout the history has evolved around understanding how to manipulate materials, although for a long time the development of new materials was slow and progress was made primarily by trial and error.

At the start of the 20th century this started to change drastically, with the formulation of the atom as we understand it today and the development of quantum mechanics. Material properties are largely dictated by the interplay of electrons with each other and with atomic nuclei, and hence they need a quantum mechanical description in order to be well understood. In the last century the manipulation of materials reached a milestone with the development of computers, which gives us the possibility to not only

expand our physical capabilities, but our mental capabilities as well. One may even refer to the current age as the age of silicon [1], which is the key material in a typical computer chip.

The rise of the computer has opened up a great number of possibilities, and it has greatly aided us in understanding the behaviour and properties of different materials, and also in the development of new ones. As computational power has gotten cheaper and more available, simulation of materials has become a more and more important tool in the search for new materials, which in turn may be used for the development of improved tools for a variety of applications. This is how we approach the actual topic of this thesis, which is an agglomeration of computational studies regarding a number of different materials. In common for these studies is that they are all concerned with two-dimensional (2D) materials, in one way or another.

A 2D material is a truly atomically thin material, consisting of one to a few layers of atoms [2,3]. The 2D morphology is intriguing from primarily two aspects: firstly, the intrinsic 2D morphology leads to novel physics and lends a 2D material properties typically different from that of the three-dimensional (3D) counterpart, and secondly, the surface area is extremely large relative to the mass or volume of the material. For the purpose of this thesis, the latter aspect is of most interest. The very high relative surface of 2D materials renders them intrinsically interesting for all applications involving surface interactions, such as catalysis, sensing, and energy storage.

In particular, different kinds of efficient energy storage is the key argument for the work presented here, be it through storage in batteries, supercapacitors, or through chemical processes (via catalysis). The human population is rising globally, as are the living standards, which indicates increased energy consumption. In order to transition away from fossil fuels, we need to harvest energy from renewable sources, such as solar, wind and water power. These energy sources all have in common that they are less flexible than fossil fuels, either by being less portable or less controllable, and thus we need powerful, efficient and sustainable means to store energy from these sources. This is our motivation for studying 2D materials.

1.1 Nanolaminated materials

Common for all 2D materials studied in this thesis is that they are synthesised, or predicted to be synthesised, by a so called top-down approach from a nanolaminated parent material. Thus, this is where the discussion will start. Nanolaminated 3D materials are characterised by exhibiting a clearly layered structure. They can be characterised by the bonding between these layers, which is either of van der Waals (vdW) or chemical bonding type.

Figures 1.1.1 and 1.1.2 show a number of nanolaminated structures from different structural families. Figure 1.1.1a)-c) shows graphite, a transition

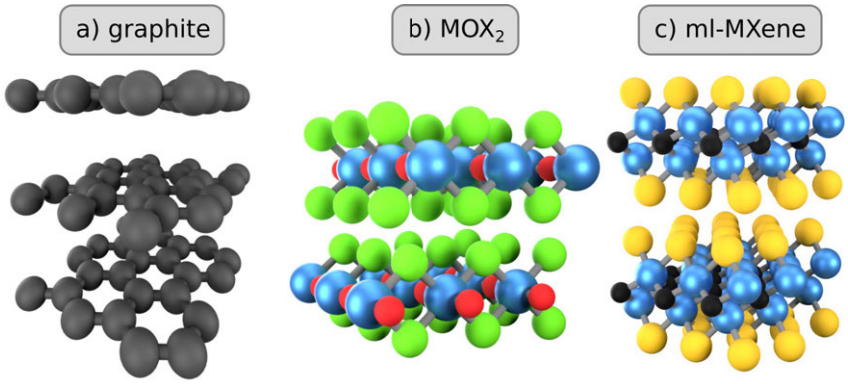

Figure 1.1.1: *Examples of different nanolaminated structures with van der Waals bonding. a) shows the carbon allotrope graphite, b) shows a transition metal oxyhalide MOX_2, and c) shows multilayer MXene.*

metal oxyhalide (MOX_2), and multilayered MXene, respectively. The 2D morphology of these structures is evident, with 2D layers well separated by seemingly empty space along the vertical direction. These are all example of vdW type structures, in which the constituent 2D units are bound together by relatively weak interlayer vdW interactions. Figure 1.1.2a)-c) instead show nanolaminated structures characterised by chemical bonding. The layered nature of these phases is still evident, but the 2D units are not as clearly separated from one another, and it is not even necessarily obvious by simple visual inspection what are the constituent units in these materials.

All structures shown in Figure 1.1.1 and 1.1.2, with the exception of graphite in Figure 1.1.1a), are examples of structures studied in this thesis. The family of materials of the prototype shown in Figure 1.1.1b), referred to as the MOX_2 structures where M is a transition metal and X is a halide, is studied in Paper IV, where ten experimentally reported and eight hypothetical members of this family are considered. The first experimentally reported member was discovered in the 1960s[4]. Depending on the specific M-species, the structure shown in Figure 1.1.1b) is subject to different distortions, which leads to very different properties between the different members of the MOX_2 family. Although an old family of phases, not much attention has been paid to these structures until the last five years or so, when the 2D community started studying them[5–8]. A number of intriguing optical and electronic properties have since been found in the 2D versions of these phases[7,9,10], although studies have primarily been limited to computational perspectives.

Paper III primarily concerns different compositions on the vdW prototype structure shown in Figure 1.1.1c), but to a lesser extent also on the so

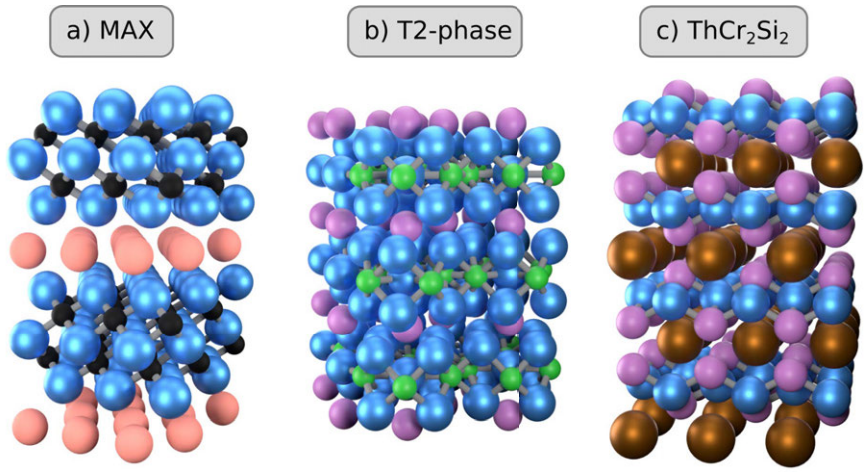

Figure 1.1.2: *Examples of different nanolaminated structures with chemical interlayer bonding. a) shows a MAX phase, b) a type of MAB phase called T2 phase, and c) a $ThCr_2Si_2$ prototype phase.*

called MAX structure shown in Figure 1.1.2a). The MAX structures, where M represents a transition metal, A an "A-element" (commonly a metalloid) and X is carbon, nitrogen, or in a few cases boron or phosphor, are a large group of structures which consists of $M_{n+1}X_n$ slabs (n being an integer) interleaved with single atom layers of A-elements[11]. For the MAX prototype in Figure 1.1.2a), $n = 2$. The structures in Figure 1.1.1c) and 1.1.2a) were both first reported in the middle of the last century[12,13], just like the MOX_2 structures. The family of MAX phases was enthusiastically expanded during the 1960, and then very little happened until 1996[11], when the MAX phases were "rediscovered", and shown to exhibit a set of interesting material properties, being both thermally and electrically conducting like a metal, but also relatively stiff and easily machinable like graphite and corrosion resistant like a ceramic[14]. The family of MAX phases is to this day a very active research area, partially because of their potential as parent structures for the synthesis of 2D materials, which will be addressed further in the next section.

Figure 1.1.2b) and c) show yet two additional chemically bound nanolaminated structures. In b) is a so called MAB phase, named thus in homage to the MAX phases. The B in MAB stands for boron, which is a common element for all MAB phases. In contrast to the MAX phases, the structure of a MAB phase is not well defined, but they consist of a number of different structural families[15]. The MAB phases are particularly intriguing

because of the inclusion of boron, which is a very diverse element. Boron has five different pure elemental phases, and binary transition metal borides are known to exhibit high hardness, having applications as hard coatings within tool manufacturing. The specific structure in Figure 1.1.2b) is a so called T2 phase[16,17], which are studied in paper I. The last structure in Figure 1.1.2c) is of the $ThCr_2Si_2$ prototype[18], which is considered in Paper V for 300 different hypothetical and reported chemical compositions. This prototype is experimentally reported in $\sim$ 700 different compositions, and display a rich palette of physical properties with, e.g., superconductivity, heavy fermions, and structural phase transitions[19].

Thus, we conclude this section noting that nanolaminated structures constitute a diverse group of materials, with attractive and interesting properties in and by themselves. However, for the purpose of this thesis, we are primarily interested in them from the perspective of synthesising 2D materials, which is the next topic of this introduction.

1.2 Removing a dimension

The field of 2D materials took flight with the realisation of graphene in 2004 – a 2D carbon allotrope of only a single atom's thickness with intriguing electronic properties[2]. Graphene was soon followed by other 2D materials, e.g. 2D transition metal dichalcogenides (TMDs) which consist of a transition metal layer decorated with chalcogens (S, Se or Te)[20], and hexagonal boron nitride (h-BN)[21].

At the start of this century, 2D materials were conceptually intriguing to the research community partially because of their absence in freestanding form. At this time, 0D and 1D quasi structures in the form of cage molecules (i.e. fullerenes for carbon) and nano tubes were realised, in addition to traditional 3D bulk structures[22]. However, no freestanding 2D phases were known of, and they were even speculated to be universally unstable[21,23], until graphene was realised by mechanical exfoliation of single or few atomic layers from 3D bulk graphite[2]. Novoselov et al. gives in ref. 22 a brief discussion on why graphene was not discovered earlier, despite the simplicity of their exfoliation method and several earlier reports on thin flakes of graphite:

1. Although the exfoliation method did consistently yield monolayer flakes, thicker flakes were in great majority.

2. 2D crystals are harder to detect in transmission electron microscopy (TEM) than, e.g., nanotubes.

3. Monolayer graphene is optically transparent, and thus hard to detect in an optical microscope.

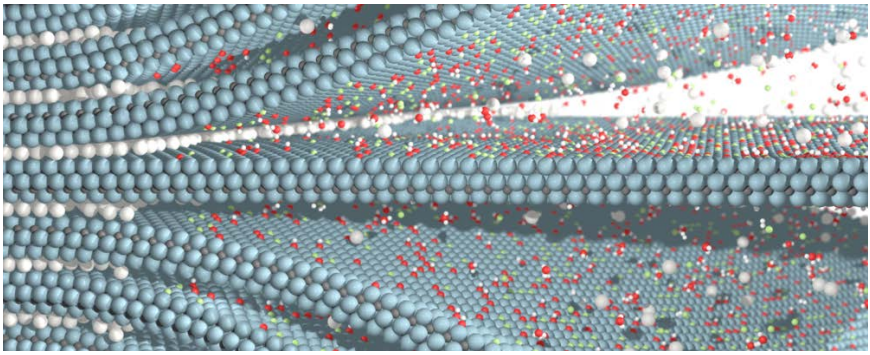

Figure 1.2.1: *Schematic illustration of the etching of a M_3AX_2 phase into M_3X_2 MXene in HF acid. Reprinted from ref. 24 with permission from the authors.*

4. Atomic force microscopy (AFM) which, at least at the time, was the only method for definitive detection of monolayer crystals has too low throughput to scan at random.

5. 2D materials were suspected to not even exist.

The key that let Novoselov et al. discover monolayer graphene despite these obstacles was that the flakes are indeed optically detectable when placed on an oxidised Si wafer[22].

Just as graphene is exfoliated from bulk graphite by mechanical means, so are many other 2D materials, e.g. *h*-BN, 2D TMDs, and 2D MOX_2 studied in Paper IV, exfoliated mechanically from their respective vdW bonded 3D parent phases[9,25]. However, to achieve successful results with mechanical exfoliation, the interlayer bonding of the 3D bulk structure needs to be sufficiently weak, rendering this exfoliation method inefficient for laminated materials with interlayer bonding of chemical type. I.e., neither of the structures in Figure 1.1.2a)-c) can be exfoliated mechanically[26,27]. Fortunately, another technique was discovered with the realisation of the first 2D MXene. In 2011 Naguib et al.[3] managed to exfoliate a MAX phase, namely Ti_3AlC_2, schematically represented by the structure in Figure 1.1.2a), into a 2D material by a completely new exfoliation method. In this method, referred to as chemical exfoliation or selective etching, the A-layers of the parent MAX phase are selectively etched away, by chemically breaking the M-A bonds which are relatively weak compared to the M-X bonds[28]. Depending on which MAX phase is used as parent phase, a successful etching process results in a 2D material of structure $M_{n+1}X_n$, i.e. $n+1$ transition metal layers interleaved with n layers of X-element (C or N), where n is the same as in the parent MAX phase. The very first such material was

Ti_3C_2, and it was coined "MXene", with "MX" referring to the derivation from the MAX parent phase, and the ending "-ene" in analogy to graphene. The etching process of a M_3AX_2 phase is illustrated in Figure 1.2.1, where the MAX phase is still intact in the leftmost part of the Figure, while completely etched into M_3X_2 at the rightmost part of the Figure.

Synthesising MXene by selective etching was originally performed at room temperature with the help of hydroflouric (HF) acid, followed by sonication for further separation of the 2D sheets from one another, and finally intercalation of various ions in between the sheets to achieve complete delamination into single layer MXene. Without intercalation, hydrogen and van der Waals bonds between the MXene sheets keep them together to form multilayer MXene[29]. In 2014 Ghidiu et al. realised the exfoliation of Ti_3AlC_2[30], the same MAX phase from which Naguib et al. fabricated the very first MXene, in a mixture of LiF and HCl instead of HF acid. Not only is this procedure less hazardous by avoiding the handling of concentrated HF acid, but the process also fully delaminates the 2D flakes in one step, since the Li^+ ions are intercalated directly during etching. Since then a number of different etching chemistries have been developed, including etching in NH_4HF_2[31], molten salts and water free etching in polar organic solvents[32].

Upon etching of the A-element, different atoms and functional groups will attach to the exposed surfaces of the M-layers. These are referred to as surface terminations or terminating species, and for MXene etched in F-containing aqueous solutions they consist of F, O and OH-groups, coming primarily from the F^- and H_2O environment. This is illustrated in Figure 1.2.1 by green (F), red (O) and small white (H) atoms covering the exposed MXene surfaces. When other chemicals are used for the etching, other terminations, such as Cl and Br, have been realised[33,34]. The terminations are very important because they considerably affect the properties of the MXene[27,35].

Besides property tailoring via choice of terminating species[34], structural and compositional design of the 2D MXene via the parent MAX phase can also be used to manipulate the properties of the resulting MXene. In addition to $M_{n+1}AX_n$ structures being realised with different n leading to MXene with different numbers of M- and X-layers, mixing of different elements within the MAX parent phase, primarily on the M-site, has lead to the realisation of MXene with in- and out-of-plane ordered atomic configurations within the M-layers, disordered mixing of M-site elements, in-plane ordered and disordered M-vacancies and high entropy MXenes. A neat schematic summary of the different design possibilities for MAX and MXene can be found in the recent review of ref. 24. This tremendous number of design choices possible for MXenes lends them properties suitable for a large number of different applications, and it is thus not hard to understand

the high interest shown for this material family.

The vast majority of 2D materials synthesised via selective etching are MXenes exfoliated from a MAX phase or, in a few cases, from other MAX-like structures[24]. Nevertheless, the set of different types of 2D materials synthesised via this method is subject to active expansion. In 2021, the first free standing 2D boride – boridene – was reported by selective etching of the parent MAB structure $(Mo_{2/3}(Sc/Y)_{1/3})_2AlB_2$[36], and even more recently, $Ru_2Si_xO_y$ was reported by etching of YRu_2Si_2. These two examples constitute inspiration to the work presented in Papers II and V of this thesis. In particular, YRu_2Si_2 belongs to a family of 3D structures with over 700 members[19], alluding to a likely expansion of the single 2D $Ru_2Si_xO_y$ into a new family of chemically exfoliated 2D materials.

Chapter 2

Density functional theory

An immensely useful formulation of quantum mechanics
This chapter presents the theoretical ground on which the simulations in this thesis rest. Although all properties of a quantum system are *in principle* attainable by solving the Schrödinger equation (or in a relativistic setting the Dirac equation) and finding the wavefunction, the procedure is highly demanding and the computations quickly become too expensive to be feasible on modern hardware, or even doable. We can by straight forward solution of the Shrödinger equation only describe systems with a handful of particles, while in material science we are typically interested in systems comprised of several *moles* of *atoms*, each atom contributing with a nucleus and a number of electrons.

Just to give some perspective, say we want to investigate a piece of diamond, a cube of side 100 nm. The lattice parameter of diamond is ~ 3.6 Å, i.e. the 100 nm diamond cube fits approximately $2 \cdot 10^7$ diamond unit cells, each containing eight carbon atoms, each atom in turn consisting of one nucleus and six electrons. The number of particles in our not particularly large diamond cube is thus on the order of 10^9 particles, which is 8 orders of magnitudes more than modern computers can do in a straight forward approach of solving the Schrödinger equation.

So what do we do? Fortunately, several approximations, reformulations and simplifications have been developed, which reduce the task to a point where we can actually perform adequately accurate simulations of reasonably complex and extended systems within more or less acceptable computation time. This chapter presents the most fundamental and essential of those methods that have been used throughout this thesis.

In 1926, the Schrödinger equation was introduced,[37] describing the wave properties observed in massive particles. Two years later came its relativis-

tic counterpart, the Dirac equation. For most applications it is enough to consider the non-relativistic Schrödinger equation, which for a single particle reads:

$$i\hbar\frac{\partial}{\partial t}\psi(\mathbf{r},t) = \hat{H}(t)\psi(\mathbf{r},t). \tag{2.1}$$

The Hamiltonian $\hat{H}$ fully determines the system, which in turn is described by the wavefunction ψ. Often we are primarily interested in a system at equilibrium, in which case the time dependence of the wavefunction is trivial, and the one particle Shrödinger equation reduces to:

$$\hat{H}\psi(\mathbf{r}) = E\psi(\mathbf{r}), \tag{2.2}$$

where E is the energy of the eigenstate ψ. Equation 2.2 is referred to as the time independent Shrödinger equation, and this is the version that will be considered in the following.

The most general Hamiltonian of a regular matter system including electrons and nuclei describes the full picture of multiple interacting particles. It is written in atomic units (a.u.) as:

$$\begin{aligned}\hat{H} = &-\frac{1}{2}\sum_{i}^{N}\nabla^2_{\mathbf{r}_i} - \sum_{J}^{M}\frac{1}{2M_J}\nabla^2_{\mathbf{R}_J} \\ &+\sum_{i<j}\frac{1}{|\mathbf{r}_i-\mathbf{r}_j|} + \sum_{I<J}\frac{Z_I Z_J}{|\mathbf{R}_I-\mathbf{R}_J|} - \sum_{i,J}\frac{Z_J}{|\mathbf{r}_i-\mathbf{R}_J|}.\end{aligned} \tag{2.3}$$

The first term gives the kinetic energy of the N electrons in the described system, with $\nabla^2_{\mathbf{r}_i}$ denoting the second order derivative with respect to the electronic coordinate $\mathbf{r}_i$. The second term describes the kinetic energy for the M nuclei, each with mass M_J. On the second line are the electrostatic contributions: the first of these terms describe the electron-electron interaction, the second the interaction of nuclei with charge Z_I and Z_J, and the last term is the electron-nucleus interaction.

Equation (2.2) with the Hamiltonian from (2.3) is a complicated equation, where the number of variables quickly increases with the number of particles, and the full wavefunction solving equation (2.2) depends on the position of every particle in the system. This Schrödinger equation is in general too complicated to solve even numerically with the aid of computers, simply because of the tremendous amount of memory required. For a system of non-interacting particles, on the other hand, only the two first terms in the Hamiltonian (2.3) remain, and each particle is simply described by a single particle Shrödinger equation, where each single particle solution has only three parameters $\mathbf{r}_i = (x_i, y_i, z_i)$. Thus, it is clear that the

interactions are posing the biggest challenge in a many-body system, and that this is where the efforts should be invested in finding approximations to the many-body problem.

A commonly employed approximation is the Born-Oppenheimer (BO) approximation[38], also called the adiabatic approximation. In the BO approximation the nuclei are assumed infinitely heavy compared to the electrons, and the wavefunction can then be written as two separate parts, describing the electrons and nuclei, respectively. The electrons still feel the nuclei, but only as a stationary external potential $V_{ext}(\{\mathbf{r}\};\{\mathbf{R}\})$ which depends parametrically on the positions $\{\mathbf{R}\}$ of the nuclei. The Hamiltonian for the electrons can then be written as:

$$\hat{H}_e = -\frac{1}{2}\sum_i^N \nabla^2_{\mathbf{r}_i} + \sum_{i<j} \frac{1}{|\mathbf{r}_i - \mathbf{r}_j|} - V_{ext}(\{\mathbf{r}\};\{\mathbf{R}\}) \tag{2.4}$$

Although useful, and widely used, the BO approximation is nowhere close to removing the challenges of solving a many-body interacting system, and further simplifications are needed. One attempt was made, also during the development of the quantum mechanical theory in the 1920s, independently by Thomas and Fermi[39–41]. Instead of solving the Schrödinger equation to get the many particle wavefunction, they proposed to approximate the energy of the electrons by a functional of the particle density. A functional $f[g(x)]$ depends on $g(x)$ at all values of x, e.g. $f[g(x)] = \int g(x)dx$. They formulated this method based on the homogeneous electron gas, which proved a simplification too crude to give very useful results. However, in 1964 the concept of formulating quantum mechanics in terms of the particle density got an important addition, when Hohenberg and Kohn wrote their paper on the inhomogeneous electron gas[42]. In this essential paper they present the two Hohenberg-Kohn theorems, proven in section 2.1, which are two of the three corner stones in the extremely successful theory for studying quantum systems called density functional theory (DFT):

- **Theorem I**: For any system consisting of N interacting particles in an external potential $V_{ext}(\mathbf{r})$, the potential $V_{ext}(\mathbf{r})$ is uniquely determined by the ground state particle density $n_0(\mathbf{r})$. Since this means the Hamiltonian is determined by $n_0(\mathbf{r})$, all properties of the system are in principle determined by $n_0(\mathbf{r})$.

- **Theorem II**: A universal functional $F[n(\mathbf{r})]$ for the energy of the system can be defined, such that $F[n(\mathbf{r})]$ is valid for any external potential $V_{ext}(\mathbf{r})$, and $F[n(\mathbf{r})]$ has its global minimum at the ground state density $n_0(\mathbf{r})$.

These two theorems are indeed intriguing, but by themselves not of much use. However, together with the third corner stone of DFT, the Kohn-Sham (KS) ansatz[43], they have provided an immensely powerful theory. The KS ansatz was proposed in 1965 by Walter Kohn and Lu Jeu Sham, and it argues that if the ground state particle density $n_0(\mathbf{r})$ is what we need to characterise a system, then we can reconstruct the density $n_0(\mathbf{r})$ in a non-interacting system to model the corresponding interacting one. According to the HK theorems, a system is fully determined by its ground state density $n_0(\mathbf{r})$, thus as long as $n_0(\mathbf{r})$ is the same for any two systems, they should behave the same way. This is exactly what DFT aims to utilise, by modelling the interacting system as a non-interacting one, subjected to an effective potential. Such a non-interacting system is called a Kohn-Sham (KS) system, and is described by the Hamiltonian $\hat{H}_{KS}$:

$$\hat{H}_{KS} = -\sum_i \frac{\hbar}{2m}\nabla^2_{\mathbf{r}_i} + V_{\mathit{eff}}[n_0], \tag{2.5}$$

where the effective potential $V_{\mathit{eff}}[n_0]$ is by definition such that the KS system exactly mimics the ground state density n_0 of the corresponding interacting system. We have here and in the following dropped the explicit $\mathbf{r}$-dependence of the particle density n, to increase readability.

Although the many-body problem is conceptually greatly reduced by avoiding interactions through the KS ansatz, it is not solved since we don't yet know the form of the energy functional $F[n]$, nor do we know that there exists an effective potential $V_{\mathit{eff}}[n_0]$ that lets us use the KS ansatz in practise. Thus, some of the multiple approaches to handle these problems will be discussed in the following, along with a more detailed presentation of the basic theory of DFT.

2.1 Basic theory of DFT

The HK theorems

Following reference 44 we will argue for the Hohenberg-Kohn theorems in a rather elegant manner: Assume we have a Hamiltonian of the form:

$$\hat{H} = \hat{H}_0 + \int V_{ext}(\mathbf{r})\hat{N}(\mathbf{r})d^3\mathbf{r}, \tag{2.6}$$

where $V_{ext}(\mathbf{r})$ is an arbitrary external potential and $\hat{N}(\mathbf{r})$ is the particle charge density operator. The expectation value of $\hat{N}(\mathbf{r})$ for a normalised state ϕ is $\langle\phi|\,\hat{N}(\mathbf{r})\,|\phi\rangle = n$, which is the charge density.

We then identify the set of states, $\{|\phi_a\rangle\}$ which gives a certain density n_a. The expectation value of $\hat{H}_0$ is in general not the same for the different

states $|\phi_a\rangle$, and we denote the smallest value by

$$F[n_a] = \min(\{\langle\phi_a|\,\hat{H}_0\,|\phi_a\rangle\}) = \langle\phi_a^{min}|\,\hat{H}_0\,|\phi_a^{min}\rangle\,, \tag{2.7}$$

where the state $|\phi_a^{min}\rangle$ (or set of states $\{|\phi_a^{min}\rangle\}$) is defined as the state (or states) that minimises the expectation value of $\hat{H}_0$, i.e. that gives $F[n_a]$. The quantity $F[n_a]$ is a functional of the density n_a, indicated by the square brackets, which means that F depends on $n_a(\mathbf{r})$ at all points in space. In the discrete case, i.e. if the density is only considered at a discrete number of p points in space, F instead reduces to a function of p variables.

Further, we define the functional E as:

$$E[n_a] = F[n_a] + \int V_{ext}(\mathbf{r})n(\mathbf{r})d^3\mathbf{r}, \tag{2.8}$$

which gives the total energy for the state $|\phi_a^{min}\rangle$, i.e. $E[n_a] = \langle\phi_a^{min}|\,\hat{H}\,|\phi_a^{min}\rangle$. With E_0 denoting the ground state energy, it is easily realised that

$$E[n_a] \geq E_0, \tag{2.9}$$

since the ground state energy is per definition the lowest energy of a system. Remember that n_a is an arbitrary particle density, which in general does not coincide with the ground state particle density. Since the difference between $F[n_a]$ and $E[n_a]$ only involves the particle density n_a, which is the same for all states in the set $\{|\phi_a\rangle\}$, the state $|\phi_a^{min}\rangle$ minimising $\langle\hat{H}_0\rangle$ will also minimise the total energy $\langle\hat{H}\rangle = E[n_a]$ for the particular density n_a.

Then, we denote (one of) the ground state(s) of $\hat{H}$ by $|\psi_0\rangle$, and the density this gives rise to by n_0. We can thus write the ground state energy as

$$\begin{aligned} E_0 = \langle\psi_0|\,\hat{H}\,|\psi_0\rangle = \langle\psi_0|\,\hat{H}_0\,|\psi_0\rangle + \int V_{ext}(\mathbf{r})n_0(\mathbf{r})d\mathbf{r} \\ \geq F[n_0] + \int V_{ext}(\mathbf{r})n_0(\mathbf{r})d\mathbf{r} = E[n_0], \end{aligned} \tag{2.10}$$

where the inequality indicates that we don't know that $|\psi_0\rangle$ yields $F[n_0]$. However, the only way for equation (2.9) and (2.10) to not be contradictory is if

$$E[n_a] \geq E_0 = E[n_0]. \tag{2.11}$$

By equation (2.11) we have shown the second HK theorem: that the density that minimises the functional $F[n]$, and thus the total energy $E[n]$, is indeed the ground state density n_0.

The proof for the first HK theorem proceeds by *reductio ad absurdum*: Assume we have two different external potentials $V_1(\mathbf{r})$ and $V_2(\mathbf{r})$, which

both give rise to the same ground state density $n_0(\mathbf{r})$. Since $V_1(\mathbf{r})$ and $V_2(\mathbf{r})$ are different, the Hamiltonians $\hat{H}_1 = \hat{H}_0 + V_1(\mathbf{r})$ and $\hat{H}_2 = \hat{H}_0 + V_2(\mathbf{r})$ will also be different, and their corresponding ground states described by two different wavefunctions, $|\psi_1\rangle$ and $|\psi_2\rangle$. We can then write:

$$\begin{aligned} E_1 = \langle\psi_1|\hat{H}_1|\psi_1\rangle &< \langle\psi_2|\hat{H}_1|\psi_2\rangle = \langle\psi_2|\hat{H}_2 - \hat{H}_2 + \hat{H}_1|\psi_2\rangle \\ &= \langle\psi_2|\hat{H}_2|\psi_2\rangle + \langle\psi_2|\hat{H}_1 - \hat{H}_2|\psi_2\rangle \\ &= E_2 + \langle\psi_2|\hat{H}_0 - \hat{H}_0|\psi_2\rangle + \int [V_1(\mathbf{r}) - V_2(\mathbf{r})]\, n_0(\mathbf{r}) d^3\mathbf{r} \\ &= E_2 + \int [V_1(\mathbf{r}) - V_2(\mathbf{r})]\, n_0(\mathbf{r}) d^3\mathbf{r} \\ &\Rightarrow E_1 < E_2 + \int [V_1(\mathbf{r}) - V_2(\mathbf{r})]\, n_0(\mathbf{r}) d^3\mathbf{r}. \end{aligned} \tag{2.12}$$

In a similar manner, we can get the inequality

$$E_2 < E_1 + \int [V_2(\mathbf{r}) - V_1(\mathbf{r})]\, n_0(\mathbf{r}) d^3\mathbf{r},$$

which put together with equation (2.12) results in the inequality:

$$E_1 + E_2 < E_2 + E_1, \tag{2.13}$$

which indeed seems a bit absurd. By this contradiction, we have shown also the second HK theorem, that the external potential $V_{ext}(\mathbf{r})$ is uniquely determined by the ground state density n_0, and vice versa. The elegant thing about these proofs is that they are in no way restrictive to the particle density being the key quantity, but $\hat{N}$ can in principle be any operator that can be included in the Hamiltonian on the form given in equation (2.6).

The KS ansatz

We now move on to the KS ansatz, in which the interacting system is remodelled into an auxiliary, non-interacting system subjected to an effective potential such that the ground state density n_0 is the same as in the fully interacting system. To find the effective potential, commonly called the Kohn-Sham potential (KS potential) v_{KS}, the total energy of the fully interacting system is segmented into a number of different contributions. First, we separate the kinetic energy $T[n_0]$ into the part coming from a non-interacting system of density n_0, and the remainder which comes from the interactions: $T[n_0] = T_0[n_0] + T_{xc}[n_0]$. The rest of the energy is separated into the external energy $E_{ext}[n_0]$, coming from the interactions of the particles with an external potential (the nuclei), the Hartree energy $E_H[n_0]$, and the remainder, $\epsilon_{xc}[n_0]$. The Hartree energy is the electrostatic

energy obtained from a classical treatment of the particle charge density, without considering quantum effects such as the antisymmetry of the wave function. We can then write the total energy as:

$$E_0[n_0] = T_0[n_0] + E_{ext}[n_0] + E_H[n_0] + E_{xc}[n_0], \tag{2.14}$$

where $E_{xc} = T_{xc} + \epsilon_{xc}$. The last term, $E_{xc}[n_0]$ is what accounts for all intricate exchange and correlation effects coming from interactions between the particles besides the Hartree part, and it is referred to as the exchange-correlation energy (xc-energy). The exchange is specifically the part coming from the antisymmetry of the wavefunction.

Since the total ground state energy E_0 is a minima of the energy landscape, the variational principle asserts that any variation of $E[n]$ with respect to the density n at $n = n_0$ will be zero. Formally this reads:

$$\begin{aligned}\delta E = 0 &= \int dn \left(\frac{\delta T_0[n]}{\delta n} + \frac{\delta E_{ext}[n]}{\delta n} + \frac{\delta E_H[n]}{\delta n} + \frac{\delta E_{xc}[n]}{\delta n} \right) \Bigg|_{n=n_0} \\ &= \int dn \left(\frac{\delta T_0[n]}{\delta n} + v_{ext}[n] + v_H[n] + v_{xc}[n] \right) \Bigg|_{n=n_0}. \end{aligned} \tag{2.15}$$

Now, doing the same thing for a non-interacting system in an effective KS potential $v_{KS[n]}$, the corresponding equation would look like

$$\delta E = \int dn \left(\frac{\delta T_0[n]}{\delta n} + v_{KS}[n] \right) \Bigg|_{n=n_0}, \tag{2.16}$$

and the KS potential can by comparison of equations (2.15) and (2.16) be identified as

$$v_{KS}[n] = v_{ext}[n] + v_H[n] + v_{xc}[n]. \tag{2.17}$$

Thus the interacting system described by the Hamiltonian in equation (2.4) can equally well be modelled by the non-interacting system described by the Hamiltonian $\hat{H}_{KS} = \hat{T}_0[n] + v_{KS}[n]$, which is numerically a much simpler task. However, instead of finding the many particle wavefunction, we now need to find the xc-potential $v_{xc}[n]$, which is unfortunately a formidable task in itself.

Thus, we have proven the two HK theorems and argued for the KS ansatz, which are the fundamental parts of DFT. The theory so far is void of any approximations besides the BO-approximation, and is in principle exact for the ground state. It is however only valid for ground state systems. The next step is to formulate the KS Hamiltonian and find the ground state density, but to do so we need the xc-potential $v_{xc}[n]$, and for this approximations are in general needed.

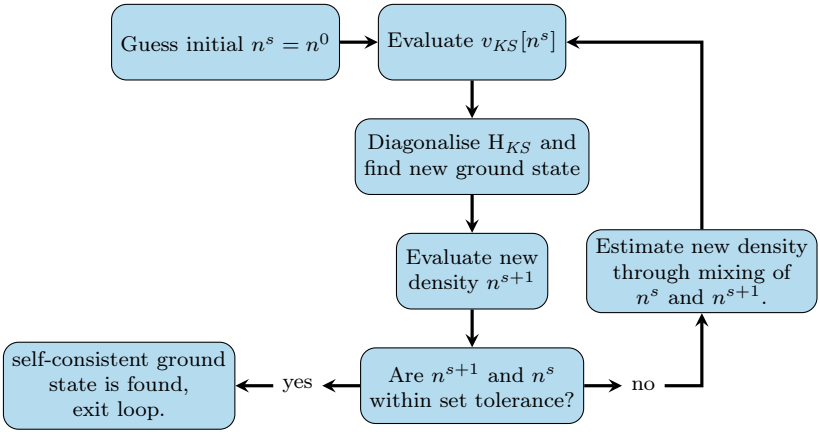

Figure 2.1.1: *Schematic of the Kohn-Sham self-consistency loop using the density as convergence criteria. In practise other criteria may be used, such as convergence of energy.*

2.1.1 The KS self-consistency loop

Once we have an expression for $v_{xc}[n]$, the full effective potential $v_{KS}[n]$ of the auxiliary system can be constructed and the KS equations solved. However, $v_{KS}[n]$ is a functional of the density n (or at least a function of n), but to get n we need to solve the KS equations, for which we need $v_{KS}[n]$. The KS equations thus need to be solved in a self-consistent manner, where $v_{KS}[n]$ is updated based on the density in each step, and vice versa.

To solve the KS equations, we start by making some initial guess for the density, n^0 where the 0 indicates the 0^{th} iteration of the self-consistency loop. The code that has been used for all calculations in this thesis, VASP, uses the atomic particle densities as n^0. From n^0 an initial $v_{KS}[n^0]$ is evaluated, and the KS Hamiltonian is constructed. Diagonalising the Hamiltonian and finding the eigenvectors gives us the KS orbitals $\phi_i^0(\mathbf{r})$ for iteration 0, from which the density is obtained as:

$$n^1(\mathbf{r}) = \sum_{occ} |\phi_i^0(\mathbf{r})|^2 \tag{2.18}$$

where the sum runs over all occupied states. Thus we have a new density n^1 from which the $v_{KS}[n^1]$ for the next step can be constructed, etc. The new density n^{s+1} is in practise not used straight off, but rather a mix of the old and new densities are used to construct the next iteration of v_{KS}, since this leads to faster convergence. The KS self-consistency loop is shown schematically in Figure 2.1.1.

2.2 The exchange correlation potential

In the KS scheme the complexity and complications of finding the ground state wavefunction is moved to finding the correct v_{KS}, which is commonly divided into the different contributions given in equation (2.17). The Hartree contribution v_H is the contribution from a classical coulomb interaction between the particles, and includes self interaction. The v_{ext} is the external potential, i.e. the nuclei as mentioned previously. The tricky part is the reminder, the exchange-correlation (xc) part v_{xc}. This part does, as the name implies, account for the exchange and correlation effects of the interactions, and it can in general not be found exactly even numerically, but must be approximated.

For the KS scheme to be useful, a good approximation for the xc-potential is required. Fortunately, the contribution from the xc-potential is in general quite small, which makes the problem somewhat easier. Exchange comes, as mentioned, from the requirement that the electronic wavefunction must be antisymmetric, and exchange can be treated exactly. However, the exchange and correlation contributions have been found to often cancel each other out, so that the total xc-potential is smaller than the exchange and correlation parts separately, and more accurate results are in general achieved when they are considered together [45,46].

2.2.1 Local and semilocal density approximations

The most straight forward, and still surprisingly useful, approximation is the local density approximation (LDA). In the LDA, instead of considering the xc-potential as a functional of n, it is simply treated as a function of n: $v_{xc}[n] \to v_{xc}(n)$. Formally, this should be a valid approximation in the limit of slowly varying densities. The actual function $v_{xc}(n)$ is derived from the homogeneous electron gas, for which the exact form of the exchange is analytically known. Different approaches has been used to approximate the correlation, which is trickier, and an accurate numerical solution was only developed in 1980 by Ceperly and Alder [47]. Modern implementations of the LDA approximation uses a parametrisation of the Ceperly and Alder correlation.

The LDA works surprisingly well for solids, even though particle densities are sometimes far from slowly varying. But of course LDA also has its shortcomings, for instance the LDA tends to overestimate chemical bonding (predicts too short bond lengths), underestimates bandgaps, and sometimes fails to resolve them all together. For chemistry purposes, where higher accuracy is needed to capture certain qualitative behaviours, LDA is in general not considered sufficient.

The most straight forward approach for trying to improve from the

LDA is to, in addition to the local density n, also consider the local density gradient ∇n. The most intuitive way to include a dependency on ∇n is to construct a systematic expansion, analogous to a Taylor series. These types of approximations for the v_{xc} are called gradient expansion approximations (GEA). Unfortunately, they do not in general improve upon the LDA, but quite often even worsens results. Instead of trying to construct an expansion based on mathematical arguments as in GEA, the expansion can be designed so that certain known properties and limiting behaviours of the exact v_{xc} are fulfilled. These approximations are called generalised gradient approximations (GGA). There are several different GGA parametrisations of the v_{xc}, and they often improve upon the LDA results. In particular they tend to soften bonding and thus compensate (though sometimes overcompensate) the overestimate of chemical bonding in LDA, and GGAs also often improve upon calculated energies[48].

One of the most well established and wide spread xc-potentials is the GGA formulated in 1996 by Perdew, Burke and Ernzerhof: the PBE functional.[48] This functional is designed to fulfil a number of known properties and limiting behaviours of the exact v_{xc} that are identified as energetically significant. It is a follow up work from earlier GGAs, and is still in wide use today, in particular within computational solid state physics. Although useful, the PBE functional still exhibits several shortcomings, e.g. it does not include van der Waals interactions, and the problem of accurately predicting material bandgaps, which is discussed further in section 2.4, largely still remains. To overcome the shortcomings of GGAs, multiple other types of approximations for v_{xc} have also been developed.

2.2.2 A van der Waals density functional

At the end of the previous century, concerns started to be raised about the inability of local and semilocal functionals – such as the popular LDA and GGA functionals – to accurately describe the long-range interactions commonly known as van der Waals (vdW) interactions, after Johannes Diderik van der Waal who first described their effects in 1873[49,50]. Claims had been presented that vdW interactions were described by some semilocal functionals, but it was later shown that the seemingly promising descriptions of certain dimers were merely coincidence. The agreement with experiments in these reports stemmed not from an accurate description of vdW interactions but was a consequence of a non-physical artefact in the exchange part of the xc-energy[46,51,52].

Van der Waals forces are due to correlation effects caused by quantum fluctuations of particle polarisations between nearby particles. Technically, these are called London dispersion forces, while vdW forces refer to several different types of electrostatic interactions. However, we choose to call them

vdW forces to be consistent with the conventions of the field. The nonlocal character of these correlation effects renders them intrinsically impossible to describe by a local or semilocal xc-functional, since they by design do not contain any nonlocal information. Thus, a density functional (DF) including vdW forces must go beyond local or semilocal approximations. There are several different approaches to how these nonlocal correlation effects may be included[46,50], out of which one of the most popular is the approach vdW-DFs and derivatives thereof, originally developed in a series of papers[51–54].

The first vdW-DF described vdW interactions between parallel sheets without atomic structure[53]. This core concept was successively developed further, first to include atomic structure by Rydberg et al.[51,54], and later to account for arbitrary geometries[52]. In the vdW-DF scheme, the correlation part of the xc-energy is divided into a local and a nonlocal part:

$$E_{xc}[n] = E_x[n] + E_c^0[n] + E_c^{nl}[n], \tag{2.19}$$

where $E_{xc}[n]$ is the full xc-energy functional, $E_x[n]$ is the exchange, $E_c^0[n]$ is the local or semilocal part of the correlation energy $E_c[n]$, and $E_c^{nl}[n]$ is the reminder which includes all nonlocal correlation effects. Thus, all vdW interactions are included in the $E_c^{nl}[n]$-part, and disregarding this part of $E_{xc}[n]$ should per definition give a result void of vdW characteristic features.

In a vdW-DF the local correlation $E_c^0[n]$ is approximated with LDA correlation $E_c^{LDA}[n]$. $E_c^{nl}[n]$, which should approach zero in the limit of a slowly varying density n, is given by the expression

$$E_c^{nl}[n] = \int_0^\infty d\mathbf{r} \int_0^\infty d\mathbf{r}' n(\mathbf{r})\phi(\mathbf{r},\mathbf{r}')n(\mathbf{r}'), \tag{2.20}$$

where $n(\mathbf{r})$ is the density at point $\mathbf{r}$, and $\phi(\mathbf{r},\mathbf{r}')$ is the so called vdW kernel. This kernel, and thus the nonlocal correlation functional $E_c^{nl}[n]$, is the same across many different vdW-DFs, although other kernels have also been proposed[55]. The original kernel is derived by assuming a dielectric response function for the vdW interactions, which is the kernel used in the vdW-DF used within this thesis. The double integral in equation (2.20) can be solved efficiently by fast Fourier transforms using the algorithm developed by Román-Pérez and Soler[56]. Indeed, a calculation using a vdW-DF functional is only marginally more expensive than one using a standard GGA functional.

With the above approximations for the correlation part of the xc-energy, the only part left to vary is the exchange, $E_x[n]$. There exists a considerable number of different vdW-DF flavors based on different choice of exchange functional, the development of which was a main focus within DFT research during the early 21$^{\text{st}}$ century. Within the work of this thesis, we have used

the vdW functional optB86b-vdW-DF to model the weakly bound layered phases studied in paper III and IV. The optB86b-vdW-DF functional was developed by Klimeš et al. in 2011[57], and uses the exchange from the B86b xc-functional[58] but with parameters reoptimised to adhere to a few constraining limits. These limits are chosen so that optB86b-vdW-DF gives good predictions for a set of benchmark systems, including both weakly bound gas dimers and ionic and covalent solids, and the optB86b-vdW-DF functional has been shown to give lattice parameters, bulk moduli, and atomisation energies similar or better that those of PBE for solid state systems in all ranges of bonding[57].

2.2.3 Hybrid functionals

As already mentioned and discussed further in section 2.4, standard DFT suffers from the so called bandgap problem[59], referring to the rather consistent underestimation of bandgaps in semiconductors and insulators. This is of course a serious problem for an electronic structure theory, and considerable efforts have been put into understanding and amending it, which is one of the motivations to the development of the so called hybrid xc-functionals. An additional and perhaps even stronger motivation than the bandgap problem came from the community of computational chemistry, where both LDA and GGAs struggle to accurately describe bond energies[46,60].

An approximation scheme for solving the Schrödinger equation that existed before DFT is the Hartree-Fock (HF) method. In the HF method, the solution to the Schrödinger equation is approximated by a Slater determinant, identified by the variational principle. By doing so, the exchange is treated exactly in HF theory, while correlation effects are completely neglected. While DFT with the LDA and GGA approximations took over as the method of choice within computational physics, corrections to the HF method remained the most reliable methods for computational chemistry[46], but come at a considerably higher computational cost than either HF or DFT[60].

As opposed to in DFT, bandgaps tend to get *over*estimated in HF theory, and thus an idea may occur: Why not create some kind of hybrid between DFT and HF to get the best out of two worlds? This highly intuitive and *ad hoc* argument is actually not vastly different from one presented in the original work introducing the concept of hybrid functionals[60], although more rigorous arguments are also presented, based on the so called adiabatic connection formula[46,60,61].

In designing a hybrid functional, the exchange part of the xc-potential is adjusted by replacing a portion of the standard DFT exchange (i.e. from LDA or some GGA flavour) with exact exchange calculated from the Kohn-

Sham orbitals[45]. One might go all the way and completely replace the DFT exchange with exact exchange. However, as already mentioned, the errors in the exchange and correlation parts of the xc-potential tends to cancel each other, and completely replacing the DFT-exchange therefore typically undermines this convenient effect[45,60]. Instead, the amount of exchange that is replaced is either optimised by fitting a mixing parameter to some benchmark data, or by *ab initio* derivation via the adiabatic connection and perturbation theory. Regardless of method, the mixing parameter is typically found to switch out 20-25% of the LDA or GGA exchange for exact exchange[61,62].

Perhaps the most popular hybrid functional in the field of materials science is HSE06, first proposed by Heyd, Scuseria and Ernzerhof at the beginning of the 21$^{\text{st}}$ century[63–66]. It is commonly used in materials science specifically for the purpose of estimating bandgaps. The functional HSE06 employs a scheme for screening the long range Coulomb potential $1/r$ by dividing it into a short range (SR) and long range(LR) part according to:

$$\frac{1}{r} = \underbrace{\frac{1-\text{erg}(\omega r)}{r}}_{SR} + \underbrace{\frac{\text{erg}(\omega r)}{r}}_{LR}, \tag{2.21}$$

where $\text{erg}(z)$ is the error function (i.e. the integral of a Gaussian from 0 to z), and ω is the screening cutoff parameter, optimised to give small errors for a number of different properties – e.g. bandgaps – for a set of benchmark systems[63,64,66].

The HSE06 exchange correlations energy, E_{xc}^{HSE06} is based on the PBE approximation, and is defined as:

$$\begin{aligned} E_{xc}^{\text{HSE06}} =& aE_x^{\text{HF,SR}}(\omega) + (1-a)E_x^{\text{PBE,SR}}(\omega) \\ &+ E_x^{\text{PBE,LR}}(\omega) + E_c^{\text{PBE}}, \end{aligned} \tag{2.22}$$

with $E_x^{\text{HF,SR}}(\omega)$ being the short ranged (SR) HF exchange, $E_x^{\text{PBE,SR}}(\omega)$ and $E_x^{\text{PBE,LR}}(\omega)$ the short and long ranged (LR) PBE exchange respectively, and E_c^{PBE} the correlation energy as taken from PBE. The parameter $a = 1/4$, which is derived from perturbation theory[62], thus specifies the portion of the PBE exchange which is replaced with the HF counterpart at short range. At long range, only the PBE exchange contributes. The division into the short and long range parts effectively introduces a screening to the HF-exchange, defining HSE06 as a screened hybrid functional.

What is considered short and long range is determined by the parameter ω, and the derivations of the three different terms $E_x^{\text{HF,SR}}(\omega)$, $E_x^{\text{PBE,SR}}(\omega)$ and $E_x^{\text{PBE,LR}}(\omega)$ can be found in the original publication[63]. In the limiting case $\omega \to \infty$ (only long range contribution) , E_{xc}^{HSE06} reduces to the usual

PBE approximation, while for $\omega = 0$ (only short range contribution), it reduces to another hybrid called hPBE or PBE0[48,62,67,68]. PBE0 does not include a cutoff criteria for the HF part of the exchange, but applies it everywhere.

The reason for the introduction of the cutoff parameter ω in HSE06, and the successive success of this functional as a go-to hybrid functional for calculating bandgaps within materials science, is because of computational feasibility. Evaluation of the HF exchange energy includes a computationally expensive integral, which generally limits the applicability of hybrid functionals to extended systems. In particular for metallic and small bandgap systems the convergence of hybrid functionals is typically very slow[63,69]. By dividing the Coulomb interaction into a short and long range part and only including the faster decaying short ranged part into the hybrid functional construction, HSE06 can be used for all kinds of electronic systems with reasonable computations times. Still, it should be noted that the computation time required to perform a bandstructure calculation with HSE06 is several orders of magnitudes larger than for PBE.

2.2.4 The modified Becke-Johnson functional

Yet another functional has been used for computing bandstructures within this thesis, namely the modified Becke-Johnsson functional (mBJ)[70,71]. This is a so called meta-GGA, which are a class of functionals that in addition to parameterising the xc-functional with respect to the local density and density gradient, also consider the kinetic energy density τ:

$$\tau = \frac{1}{2}\sum_{i=1}^{N} |\Delta\phi_i|^2,$$

where i enumerates the orbitals.

The original BJ potential is a theory for exchange only, which has been designed to mimic the behaviour of the so called Optimised Effective Potential (OEP)[72,73], but at a much lower computational cost[70]. The mBJ functional introduces a scaling factor to each of the two terms in the original BJ potential[71]. These scaling factors are both based on the parameter

$$c = \alpha + \beta\left(\frac{1}{V_{cell}}\int_{cell}\frac{|\nabla n(\mathbf{r})|}{n(\mathbf{r})}d^3r\right)^{1/2},$$

where the parameters $\alpha = -0.012$ and $\beta = 1.023$ bohr $^{1/2}$ are fitted to the bandgaps of a set of benchmark systems[71]. The mBJ functional is thus fitted individually to each system via the parameter c.

The mBJ functional is considerably cheaper computationally than any hybrid functional, screened or not. At the same time, it is claimed to

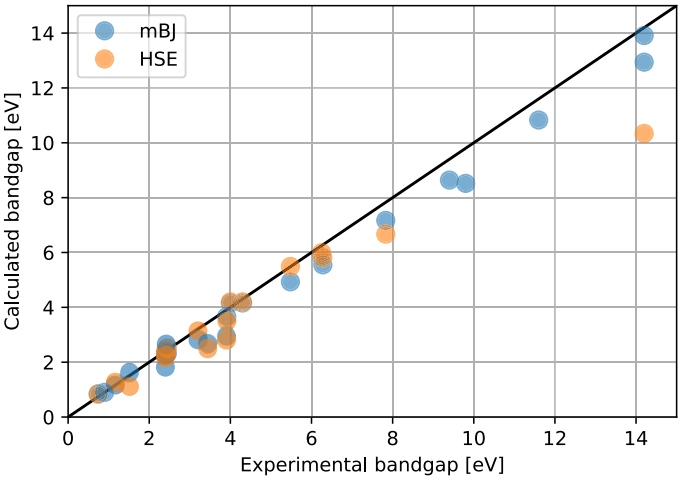

Figure 2.2.1: *Comparison of bandgaps calculated with mBJ*[71] *and HSE*[63,66] *to experimentally measured bandgaps. Data is adapted from ref. 71.*

give comparable accuracy for bandgap estimations. Figure 2.2.1 shows the bandgap as predicted with mBJ exchange (and LDA correlation) compared to the experimentally measured gap, for the set of benchmark systems used to fit α and β in the original work. The performance of the mBJ functional is clearly competitive with HSE, and even outperforms HSE in the large bandgap limit. Although, since this test specifically considers the set of structures to which mBJ was fit, one may object that this is not a fair test, but that the mBJ functional is given an artificial advantage. Nonetheless, later reports have also identified mBJ as competitive with HSE on more diverse and unbiased data sets[74]. This together with the superior computational efficiency of mBJ indeed speaks strongly in favour of the mBJ functional for calculation of bandgaps.

2.3 DFT in practise for periodic solids

When using DFT in practise there are a few things regarding the implementation one needs to pay attention to. Since the topic of this thesis is not DFT theory, but materials modelling, no attempt will be made to delve into the details of DFT implementation. However, any DFT software is strongly characterised by a few implementation choices, and thus a brief idea will be given of the background and motivation for the implementation choices characteristic of the code *Vienna Ab initio Simulation Package* –

VASP – which is the code used for the calculations in this thesis.

Firstly, one needs to choose the basis for representation of the KS system. In principle, any complete set of functions can be used to describe any system, but in practice a complete set can not actually be realised, but it needs to be truncated at some point. With this in mind, each basis set has different advantages and disadvantages and are thus used for different situations. For applications within chemistry it is common to use localised functions, such as atomic orbitals or Gaussian functions, since the systems are typically localised and limited in size. In solid state physics one typically works with periodic systems for which Bloch's theorem applies, stating that the electronic wave functions must also be periodic, and thus a plane wave (PW) basis set is arguably suitable for solid state systems. A PW basis set also makes it easy to work in Fourier space, which is quite natural when dealing with periodic solids, and facilitates certain calculations.

For solids periodic in less than three dimensions, such as the 2D phases studied in paper II, it is less obvious what basis set to choose. Since a PW basis set implies the use of periodic boundary conditions, an artificial periodicity will be introduced for any system not periodic in all three directions, which is a potential problem not only for a low-dimensional system but also for a system including disorder of any kind. However, by modelling the non-periodicity on a large enough computational unit cell, the effects of the artificial periodicity can be made small enough to be negligible. For 2D structures in particular, this typically means a vacuum spacing is introduced to the unit cell to separate the 2D sheets.

The PAW method

Although the PW basis set seems like the obvious choice for a periodic material, particularly if it is periodic in all three directions, it still comes with some complications. The core states which are tightly bound oscillate rapidly close to the core, in particular those of high angular momentum. To represent such rapidly oscillating states with plane waves, a large number of waves is needed in the basis set, making the basis inefficient for practical purposes. This is where another key piece of theory is needed: the projected augmented wave (PAW) method.[75]

The key idea of the PAW method is to replace the all electron (AE) wavefunctions ψ by the pseudised wavefunctions $\tilde{\psi}$, which are designed to coincide with ψ outside a core region where the electrons can be treated as nearly free, while inside the core region they oscillates less rapidly and are smoother than the AE wavefunctions. This division into core and interstitial regions is called a muffin tin (MT) partitioning and is commonly employed within solid state theory. The MT partitioning is schematically depicted in Figure 2.3.1. Since the pseudised wavefunctions $\tilde{\psi}$ and the AE wavefunctions ψ are the same in the interstitial region, $\tilde{\psi}$ will have the cor-

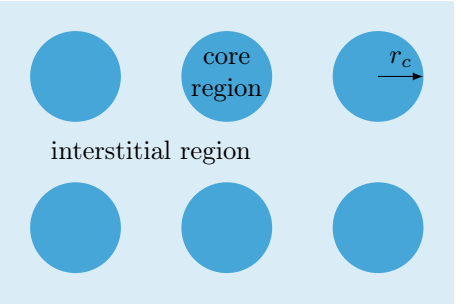

Figure 2.3.1: *The muffin tin (MT) partitioning of a lattice. The core regions, where the electrons are tightly bound to the nuclei and participate minimally in binding, are separated from the valence or interstitial region, where the electrons are nearly free.*

rect behaviour in this region. The core region is just replaced by AE core region wavefunctions of a reference system. It should be noted that "all electron" in in this context refers to the exact Kohn-Sham single particle wavefunctions, not to the many-body wavefunction.

For a more formal description, an AE wavefunction is expanded as a sum of partial waves centred at the cores:

$$|\psi\rangle = \sum_i c_i \, |\phi_i\rangle \, .$$

Similarly a pseudo wavefunction can be expanded in pseudo partial waves inside the core region:

$$|\tilde{\psi}\rangle = \sum_i \tilde{c}_i \, |\tilde{\phi}_i\rangle \, .$$

The subscript i denotes the spatial position $\mathbf{R}$, angular momentum quantum numbers l and m_l as well as a principal quantum number n. The pseudised and AE partial waves ϕ_i and $\tilde{\phi}_i$ are identical outside the core region, as are the wavefunctions ψ and $\tilde{\psi}$. The pseudised and all electron Hilbert spaces are related to each other thorough a linear transform: $|\psi\rangle = \mathcal{T} \, |\tilde{\psi}\rangle$, and $|\phi_i\rangle = \mathcal{T} \, |\tilde{\phi}_i\rangle$. Hence the expansion coefficients c_i and $\tilde{c}_i$ are identical, and are written

$$c_i = \langle \tilde{p}_i | \tilde{\psi} \rangle \, ,$$

where $\tilde{p}_i$ are called projector functions. They have the property $\langle \tilde{p}_i | \tilde{\phi}_j \rangle = \delta_{ij}$. Hence, the complete transform of an AE wavefunction is written as:

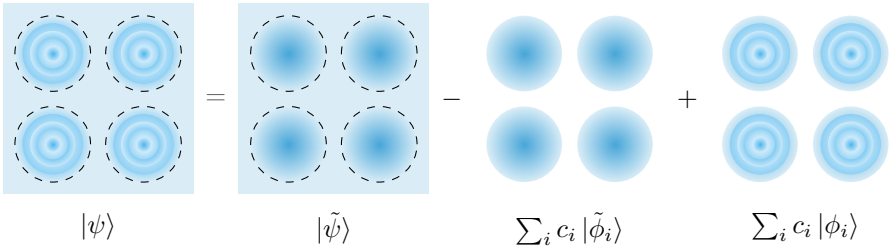

Figure 2.3.2: *Schematic illustration of the PAW method: the AE wavefunction $|\psi\rangle$ is constructed from the pseudo wavefunction $|\tilde{\psi}\rangle$ by subtracting the partial wave expansion of $|\tilde{\psi}\rangle$, $\sum_i c_i |\tilde{\phi}_i\rangle$, inside the core region and replacing it by the partial wave expansion of the AE wavefunction, $\sum_i c_i |\phi_i\rangle$. The latter is determined from a reference system, e.g. free atoms.*

$$\begin{aligned} |\psi\rangle &= \mathcal{T}|\tilde{\psi}\rangle = \sum_i c_i \mathcal{T}|\tilde{\phi}_i\rangle = \sum_i c_i |\phi_i\rangle + |\tilde{\psi}\rangle - |\tilde{\psi}\rangle \\ &= |\tilde{\psi}\rangle + \sum_i c_i |\phi_i\rangle - \sum_i c_i |\tilde{\phi}_i\rangle \\ &= |\tilde{\psi}\rangle + \sum_i \left(|\phi_i\rangle - |\tilde{\phi}_i\rangle\right) \langle \tilde{p}_i | \tilde{\psi}\rangle \,. \end{aligned} \tag{2.23}$$

Equation (2.23) describes how an AE wavefunction ψ is constructed from the corresponding pseudo wavefunction $\tilde{\psi}$, by cutting away the core region where ψ and $\tilde{\psi}$ are different and replacing it with the AE solution. Most commonly, though not necessarily, this is done within the frozen core approximation, meaning the core states are assumed stationary and unaffected by the valence electrons. A graphical interpretation of equation (2.23) is shown in Figure 2.3.2.

2.4 The bandgap problem of DFT

One of the most well known shortcomings of DFT is the so called bandgap problem, which refers to the failure of DFT in predicting accurate electronic bandgaps. The fundamental bandgap Δ is defined as the difference in the ionisation energy I and electron affinity A, where N is the total number of electrons in the system:

$$\Delta = I - A = (E[N-1] - E[N]) - (E[N] - E[N+1]) \,. \tag{2.24}$$

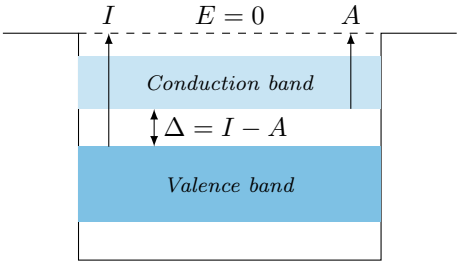

Figure 2.4.1: *Schematic illustration of the fundamental bandgap in an insulating or semiconducting material.*

The bandgap Δ is a function(al) of ground state properties, since all energies in equation (2.24) are ground state energies. Thus the bandgap is in principle a ground state property and should be attainable from KS theory. However, the bandgap Δ as given in equation (2.24) is a bit tricky to evaluate computationally in extended systems, i.e. in systems exhibiting band structure. These systems are in practise treated using periodic boundary conditions, and in such a description it is impossible to add or remove a single electron, which is required to evaluate I and A as given in equation (2.24).

The bandgap can also be defined as the difference between the highest occupied energy level, ϵ_{HO} and the lowest unoccupied level, ϵ_{LU}. For the KS system the bandgap could then be given by:

$$\Delta_{KS} = \epsilon_{LU} - \epsilon_{HO}, \tag{2.25}$$

where the energies ϵ are the KS single particle eigenvalues. However, through this formulation the bandgap is an excited state property, and since and there is no reason to believe the KS eigenvalues correlate with the real eigenvalues, excited state properties are not guaranteed to be correctly given by KS theory even for the exact v_{KS}. The only KS eigenvalue which has been found to have a physical meaning in itself is that of the highest occupied orbital, which is the negative ionisation energy: $\epsilon_{HO} = -I$. Hence the bandgap Δ_{KS} can only be used to approximate Δ if $\Delta_{KS} = \Delta$ for exact KS theory. However, it can be shown that this is not the case, since the exact xc-energy may exhibit non-smooth behaviour at integer particle densities. More specifically, with $\omega \to 0$ being an infinitesimally small number, N the total number of particles and other quantities specified by equation (2.14), it is possible to write:[59]

$$
\begin{aligned}
I - A &= \left.\frac{\delta E}{\delta n(\mathbf{r})}\right|_{N+\omega} - \left.\frac{\delta E}{\delta n(\mathbf{r})}\right|_{N-\omega} \\
&= \left(\left.\frac{\delta T_0}{\delta n(\mathbf{r})}\right|_{N+\omega} - \left.\frac{\delta T_0}{\delta n(\mathbf{r})}\right|_{N-\omega}\right) + \left(\left.\frac{\delta E_{xc}}{\delta n(\mathbf{r})}\right|_{N+\omega} - \left.\frac{\delta E_{xc}}{\delta n(\mathbf{r})}\right|_{N-\omega}\right) \\
&= \Delta_{KS} + \Delta_{xc} = \Delta. \qquad (2.26)
\end{aligned}
$$

Hence, the KS bandgap Δ_{KS} inherently lacks the part of the fundamental bandgap Δ coming from the discontinuity in the exchange correlation energy, Δ_{xc}, so that even in exact KS theory, the xc-discontinuity Δ_{xc} would need to be added to Δ_{KS} to get Δ.

The LDA and most GGA approximations do not display this discontinuity at integer particle densities, and it is thus intrinsically impossible to attain a good approximation for the fundamental bandgap from these approximations, but the best we can achieve is a good estimate of Δ_{KS}. As discussed in chapter 2.2, there are xc-potentials designed to mitigate the bandgap problems of DFT by different approaches. For example meta-GGAs (which consider the KS kinetic energy as a fitting parameter in addition to the density and density gradient) and hybrids (which substitutes part of the KS exchange with exact exchange). However, because these alternative functionals experience other shortcomings, e.g., increased computation time, GGAs are still widely employed.

Chapter 3

Stability analysis

Having solved the KS equations, the electronic structure is known for the specific external potential v_{ext}, i.e., the specific arrangement of nuclei considered. However, the solution says nothing about whether the specific v_{ext} considered actually corresponds to an arrangement of nuclei which can be realised experimentally, outside of the computer. Ultimately, we are not interested in fictitious materials that we can only study in the computer, because ultimately we are aiming at understanding and manipulating the real world around us. Although fictitious toy systems may be very instructive on our way to connect theory with reality, we typically need to consider real systems within the field of material science. Hence, we need to know whether the systems we simulate can actually be expected to be possible to synthesise in the real world, or whether they are unlikely to be found outside of the computer.

The only way to truly establish the existence of a system, or a material, is of course to realise it experimentally. However, there are theoretical tools that can be used to predict the stability of a material, and thus imply the sensibility, or futility, in trying to synthesise the simulated system. This chapter will address some of these tools.

3.1 Lattice dynamics in the harmonic approximation

At any temperature above absolute zero, i.e., any temperature of any interest for actual applications or even just synthesis, the atomic nuclei in any compound are not static, but vibrating. Hence it is important that the nuclei are all in a potential minimum of their surroundings, or the vibrations would cause the structure to quickly fall apart. The most common,

and most simple, way to model the lattice potential is by considering each lattice site as being trapped in a generalised harmonic potential. For most structures this approximation is enough to evaluate the dynamical stability, i.e. stability with respect to lattice vibrations. There are structures for which the harmonic approach is not enough, but for the purpose of this thesis we have kept within the harmonic approximation for lattice vibrations, which will be described in this section.

3.1.1 The harmonic approximation

The lattice potential $\Phi(\{u\})$ can be expanded as a Taylor series, where $u_{ni\alpha}$ is the displacement of the ith atom in the nth unitcell in the direction α ($\alpha = x, y, z$):

$$\Phi(\{u\}) = \Phi_0 + \sum_{ni\alpha} \underbrace{\frac{\partial \Phi(\{u\})}{\partial u_{ni\alpha}}}_{\Phi_{ni\alpha}} u_{ni\alpha} + \frac{1}{2} \sum_{ni,mj} \sum_{\alpha,\beta} \underbrace{\frac{\partial^2 \Phi(\{u\})}{\partial u_{ni\alpha} \partial u_{mj\beta}}}_{\Phi^{mj\beta}_{ni\alpha}} u_{ni\alpha} u_{mj\beta} + \dots \tag{3.1}$$

The 0th order term in equation (3.1), Φ_0, is simply a constant and is of no physical interest to the present discussion. The first order term $\Phi_{ni\alpha}$ is the force exerted on the lattice site indexed by (ni) upon an infinitesimal displacement in the direction α. Since the expansion is around a stationary point, this force is simply zero. The second order terms are the first important terms in this expansion, and are referred to as the "force constants" or "coupling constants". They are the analogue of the spring constant of a 1D harmonic oscillator, and serve to generalise the concept of the harmonic potential to a system with multiple degrees of freedom. Consideration of up to second order while neglecting higher order terms is thus referred to as the harmonic approximation for lattice dynamics. Using the analogue of a 1D harmonic potential, the quantity $-\Phi^{mj\beta}_{ni\alpha} u_{mj\beta}$ is the force exerted on the nucleus indexed by (ni) in the direction α upon a displacement $u_{mj\beta}$ of the nucleus indexed by (mj) in the direction β.[76]

3.1.2 Dynamical stability

The total lattice potential, $\Phi(\{u\})$ in equation (3.1), must be in a local minimum for a structure to be stable. Hence, we can deduce the stability of a structure with respect to displacements of lattice sites by studying the

total energy. This is done through the evaluation and study of the phonon spectra, the concept of which is outlined in the following.

First, we start by rewriting equation (3.1) in a more convenient matrix form, omitting the 0^{th} and first order terms:

$$\Phi(\{\mathbf{u}\}) = \frac{1}{2} \sum_{ni,mj} \mathbf{u}_{ni} \mathbf{\Phi}_{ni}^{mj} \mathbf{u}_{mj}, \tag{3.2}$$

where now $\mathbf{u}_{ni}$ are three dimensional vectors, and $\mathbf{\Phi}_{ni}^{mj}$ are the 3 by 3 force constant matrices which are elements of the Hessian matrix of the total lattice potential $\Phi(\{\mathbf{u}\})$. If $\Phi(\{\mathbf{u}\})$ is to have a minimum at $\{\mathbf{u}\} = \mathbf{0}$, the eigenvalues of the Hessian matrix must be positive definite, in analogy with the so called "second derivative test" in 1D calculus.

The equation of motion can now be written down for each atom i with mass M_i as:

$$M_i \ddot{\mathbf{u}}_{ni} = -\sum_{mj} \mathbf{\Phi}_{ni}^{mj} \mathbf{u}_{mj}. \tag{3.3}$$

As usual, since we are working with a periodic system, the plane wave ansatz for the solution to $\mathbf{u}_{ni}$ is used to simplify the equations:

$$\mathbf{u}_{ni} = \frac{1}{\sqrt{M_i}} \mathbf{u}_i(\mathbf{q}) e^{i(\mathbf{q}\cdot\mathbf{r}_n - \omega t)}, \tag{3.4}$$

where $\mathbf{r}_n$ is the position vector of the unit cell n, ω is the angular frequency and $\mathbf{q}$ is the wave vector. Inserting equation (3.4) into (3.3) yields:

$$\begin{aligned} -\omega^2 \sqrt{M_i} \mathbf{u}_i(\mathbf{q}) e^{i(\mathbf{q}\cdot\mathbf{r}_n - \omega t)} &= -\sum_{mj} \mathbf{\Phi}_{ni}^{mj} \frac{\mathbf{u}_j(\mathbf{q})}{\sqrt{M_j}} e^{i(\mathbf{q}\cdot\mathbf{r}_m - \omega t)} \iff \\ \omega^2 \mathbf{u}_i(\mathbf{q}) &= \sum_j \underbrace{\sum_m \frac{\mathbf{\Phi}_{ni}^{mj}}{\sqrt{M_i M_j}} e^{i\mathbf{q}(\mathbf{r}_m - \mathbf{r}_n)}}_{\mathbf{D}_i^j(\mathbf{q})} \mathbf{u}_j(\mathbf{q}). \end{aligned} \tag{3.5}$$

The matrices $\mathbf{D}_i^j(\mathbf{q})$ are elements of what is known as the dynamical matrix. From symmetry considerations, the dynamical matrix can be shown to be Hermitian. This is easily realised by studying the elements $\mathbf{D}_i^j(\mathbf{q})$: For the second order derivatives we have that $\mathbf{\Phi}_{ni}^{mj} = \mathbf{\Phi}_{mj}^{ni}$, since the potential energy $\Phi(\{\mathbf{u}\})$ is a smooth function of all variables $\mathbf{u}_{ni}$. Then we have:

$$\mathbf{D}_i^j(\mathbf{q}) = \sum_m \frac{\mathbf{\Phi}_{ni}^{mj}}{\sqrt{M_i M_j}} e^{i\mathbf{q}(\mathbf{r}_m - \mathbf{r}_n)} = \sum_n \frac{\mathbf{\Phi}_{mj}^{ni}}{\sqrt{M_j M_i}} e^{-i\mathbf{q}(\mathbf{r}_n - \mathbf{r}_m)} = \overline{\mathbf{D}_j^i(\mathbf{q})}, \tag{3.6}$$

where $\overline{x}$ denotes the complex conjugate of x. That the dynamical matrix is Hermitian means the eigenvalues ω^2 must be positive. Thus ω must be real, which can be used to check the dynamical stability of a structure. By finding the square root of the eigenvalues $\sqrt{\omega^2} = \omega(\mathbf{q})$ to the dynamical matrix, which are also the frequencies of the vibrational normal modes of the system, it can be determined whether the total crystal potential $\Phi(\{\mathbf{0}\})$ is at a minimum with respect to displacements $\mathbf{u}$. If all frequencies are real, we are indeed at a minimum, while if there are any imaginary frequencies this indicates a saddle point of some kind.

3.1.3 Force constants sum rules

Some properties of the crystal potential, and thereby the expansion coefficients – i.e., the force constants – can be derived by considering the symmetries of a crystal. In particular, the crystal potential must be invariant under any translational, rotational or mirror transformation. In addition, some force constants must be identical from consideration of lattice symmetries, and any permutation of the indices must also leave them unchanged, since

$$\frac{\partial^2 f(x,y)}{\partial x \partial y} = \frac{\partial^2 f(x,y)}{\partial y \partial x} \tag{3.7}$$

for a smooth, well-behaved function.

Invariance with respect to translational transformations, meaning the crystal is unaffected by any uniform displacement of all its constituent atoms, leads to the conclusion that for each set of cartesian coordinates α, β we have the translational sum rule:

$$\sum_{mj} \Phi_{ni\alpha}^{mj\beta} = 0. \tag{3.8}$$

The crystal is also invariant with respect to rotational transformations of the whole crystal, which gives other, slightly more complicated sum rules. A discussion of these can be found e.g. in ref. 77 or 78, and will not be repeated here for lack of an intuitive interpretation of the equations. It is also known that an unstrained 2D structure of one or a few layer's thickness will have a quadratic phonon branch at long wavelengths (i.e. at the Γ-point),[79] unlike the linear behaviour observed in the 1D linear chain and different 3D phases.

The sum rules are often not fulfilled by raw force constants data as obtained from *ab initio* calculations, leading to nonphysical behaviour of the long wavelength modes[79]. Hence, careful post-processing of the force constants might be necessary in order to attain a proper physical behaviour,

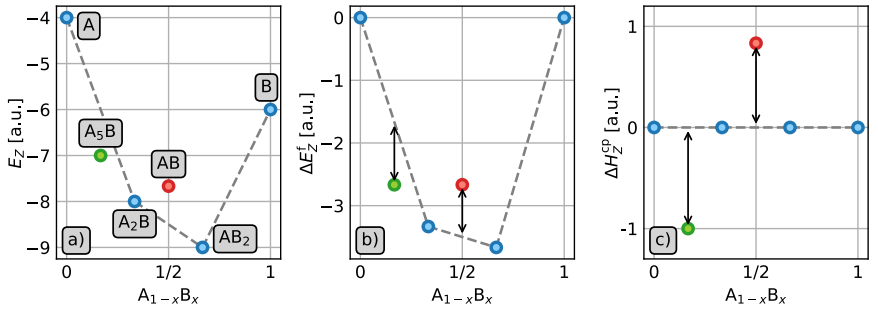

Figure 3.2.1: *Schematic illustration of the difference between the a) internal energy E_Z, b) formation energy ΔE_Z^f and c) formation enthalpy with respect to competing phases H_Z^{cp}, for different phases denoted by Z in a fictitious binary system of species A and B. The phases considered as competing phases when evaluating H_Z^{cp} are indicated in blue.*

which has been taken into consideration when evaluating the phonon spectra presented in the supporting material of paper II.

3.2 Thermodynamical phase stability

Even if a particular structure – or phase – Z, is dynamically stable, there may be other phases or combinations of phases with the same stoichiometry, i.e. the same elemental ratios, which are thermodynamically preferred. This would leave the particular phase Z energetically unfavourable and thus unlikely to form. Hence, when theoretically evaluating the possibility for a phase to form experimentally, its thermodynamical stability must be considered by comparison with other phases or combinations or phases with the same total stoichiometry.

For the purpose of evaluating thermodynamical stability, the Gibb's free energy of the phase is considered:

$$G = E - TS + pV = H - TS, \tag{3.9}$$

where T is temperature, S in entropy, p is pressure, V is volume and $H = E + pV$ is the enthalpy. E is the total internal energy, as attained from the DFT calculation. Since DFT calculations are performed at zero pressure, the pV-term is simply disregarded. Considering atmospheric pressure, 101.3 kPa, in the appropriate units we find that:

$$101.3 \text{ kPa} = 101.3 \cdot 10^3 \text{ J/m}^3 \leq 10^{-6} \text{ eV/Å}^3. \tag{3.10}$$

This is a small number, and its impact on the Gibb's free energy G is negligible. However, when considering a phase at very high external pressure, the pV-term does matter and needs to be considered. Since the DFT calculations are also performed at zero temperature, and hence $TS = 0$, the ground state Gibb's free energy G attained from the calculation equals the enthalpy H, which is just the internal energy E since we are disregarding the pressure term. The energy E, taken from the DFT calculation, is in general considered per unit cell, formula unit or atom. Thus any other terms are scaled to the same units as E. For the reminder of this discussion, energies will be assumed to be per atom.

The thermodynamical stability of a phase Z is evaluated through the formation enthalpy with respect to competing phases, ΔH_Z^{cp}. However, to facilitate the discussion, we will start by introducing another concept, namely the formation Gibb's free energy ΔG_Z^{f}. Because of the arguments given above, this is reduced to the formation energy ΔE_Z^{f}, which we will consider for the rest of this discussion. The energy for a number of phases $\mathrm{A}_x\mathrm{B}_y$ in a fictitious binary system of elemental species A and B is shown in Figure 3.2.1a). The formation energy $\Delta E^{\mathrm{f}}_{\mathrm{A}_x\mathrm{B}_y}$ of the phase $\mathrm{A}_x\mathrm{B}_y$ (x+$y = 1$) is defined by:

$$\Delta E^{\mathrm{f}}_{\mathrm{A}_x\mathrm{B}_y} = E_{\mathrm{A}_x\mathrm{B}_y} - xE_{\mathrm{A}} - yE_{\mathrm{B}}, \tag{3.11}$$

where E_{A} and E_{B} are the energies per atom of the pure elements A and B, respectively, in their most stable elemental forms. ΔE_Z^{f} is shown for the fictitious binary A-B system in Figure 3.2.1b). Comparison with Figure 3.2.1a) shows that ΔE_Z^{f} is shifted relative to E_Z by the line connecting the points corresponding to E_{A} and E_{B}. The formation energy ΔE_Z^{f} has been, and still is sometimes, used as an argument for the thermodynamical stability of a phase Z. However, all it actually describes is whether the formation of a compound $Z = \mathrm{A}_x\mathrm{B}_y$ is preferred over formation of the elemental phases A and B.

Rather than only considering pure elemental phases, it is more appropriate to compare the formation of a compound to all other phases in the appropriate compositional space[80]. Thus we define the formation enthalpy with respect to competing phases, ΔH^{cp}, which for the fictitious phase $\mathrm{A}_x\mathrm{B}_y$ is defined as:

$$\Delta H^{\mathrm{cp}}_{\mathrm{A}_x\mathrm{B}_y} = E_{\mathrm{A}_x\mathrm{B}_y} - \min\left(\sum_Y x_Y E_Y\right), \tag{3.12}$$

where x_Y is the fraction of phase $Y = \mathrm{A}_i\mathrm{B}_j$, chosen so that the sum in the last term is minimised given the stoichiometry of $\mathrm{A}_x\mathrm{B}_y$. $\Delta H^{\mathrm{cp}}_{\mathrm{A}_x\mathrm{B}_y}$ is shown for two hypothetical phases of the A-B system, $\mathrm{A}_5\mathrm{B}$ and AB, in Figure 3.2.1c). The four phases indicated by blue markers have been considered

as competing phases. AB is found to have $\Delta H^{\mathrm{cp}}_{\mathrm{AB}} > 0$, which indicates thermodynamical instability, since a lower total energy is attained from decomposing AB into A_2B and AB_2. For the hypothetical phase A_5B, on the other hand, $\Delta H^{\mathrm{cp}}_{\mathrm{A_5B}} < 0$, which indicates thermodynamical stability, since decomposition into other phases does not lower the total energy. However, Figure 3.2.1b) shows that both AB and A_5B has the same formation energy. It has been shown multiple times that stability predictions using ΔH^{cp}_Z has a strikingly better correlation with experimentally realised phases than predictions using ΔE^{f}_Z [80,81].

Equation (3.12) can be visually interpreted as the shifting of energies in Figure 3.2.1a) so that the grey dashed lines coincide with zero, as in Figure 3.2.1c). However, for illustration purposes it is more common to visualise ΔE^{f}_Z, shown in Figure 3.2.1b), than E_Z, since a large energy difference between the A and B elements would make a) hard to read. Considering ΔE^{f}_Z rather than E_Z, equation (3.12) would read:

$$\Delta H^{\mathrm{cp}}_{\mathrm{A}_x\mathrm{B}_y} = \Delta E^{\mathrm{f}}_{\mathrm{A}_x\mathrm{B}_y} - \min\left(\sum_Y x_Y \Delta E^{\mathrm{f}}_Y\right), \tag{3.13}$$

which is equivalent to the formulation in equation (3.12).

Although only discussed here for binary systems, and most easily visualised for those, the thermodynamical stability arguments presented are applicable to systems of arbitrary number of elemental species. The visualisation of larger systems does, however, get challenging quickly.

3.2.1 Stability at finite temperatures

At finite temperature, the entropy term $-TS$ is no longer automatically zero, and there are other contributions to the Gibb's free energy than just the internal energy.

The energy E and entropy S can be divided into electronic, vibrational, configurational and magnetic contributions. Magnetism is not a central aspect of this thesis, and effects from magnetic entropy has not been considered. The electronic and vibrational contributions has also been disregarded; by assuming them to be similar between different phases, they can be argued not relevant for stability analysis since we are only interested in differences between energies. Then the zero temperature formation enthalpy with respect to competing phases, ΔH^{cp}, will be characteristic for the system also at finite temperature, i.e. at synthesis conditions. That the electronic and vibrational temperature effects cancel between phases is not something that is guaranteed, but has been shown to be the case for a typical set of MAX phases,[82,83] and has provided accurate predictions for several other systems.[80,84] Hence the following discussion will only consider the configurational aspects of finite temperature.

For a perfectly ordered solid, there is only a single way to arrange the atoms, and thus the number of possible microstates for the N atoms in the solid is $g(N) = 1$ and the entropy

$$S = k_B \ln g(N) \tag{3.14}$$

is zero. Assuming all temperature effects besides entropy are disregarded, G_Z of a perfectly ordered phase is thus not affected by temperature.

For a disordered solid, with elements A and B mixed at concentrations x and $(1 - x)$ respectively, the number of possible microstates for the N atoms is instead $g(N) = N!/(n!(N - n)!)$ where $n = Nx$. This is readily extended to alloying of more than two elements, and gives in the mean field approximation, together with Sterling's approximation, the expression for the configurational entropy as:

$$S = -k_B \sum_i x_i \ln x_i \tag{3.15}$$

per atom. In a phase where only some sites are considered for alloying, e.g. a MAX phase with alloying on the M site, S is per alloying site. Since S is positive ($x_i < 1$), the configurational entropy term $-TS$ will decrease G_Z as temperature increases, thus favouring structures with disorder.

3.3 Modelling disordered structures

One of the challenges in solid state simulations is to account for structural disorder. The DFT formulation used throughout this thesis is based on the periodicity of crystalline solids, for which Bloch's theorem is valid and the system is conveniently described using a plane wave basis set and periodic boundary conditions. However, there are many materials which are not perfectly crystalline solids, and thus special care needs to be taken when dealing with those.

Disorder in this thesis is not a very central point, but it is considered in some aspects and hence this section will give a brief introduction on the method that has been used. Disorder in materials modelling refers in general to structures which exhibit a basic crystalline structure with some level of disorder incorporated on certain or all sites. Strictly within the scope of this thesis, disorder has been considered only for the terminations on boridene in paper II. In close relation however is ref. 84 – where Ti_4MoSiB_2 studied in paper I was first reported – and also ref. 85. Ref. 84 studies the phase stability of different quaternary T2 phases with ordered or disordered alloying on the M sites in the model ternary T2 phase M_5SiB_2, and in ref. 85 disorder was considered for vacancy formation in $Sc_2Al_2C_3$.

As with most phenomena there are different ways to model disorder. Herein the special quasirandom structure (SQS) method has been used,[86] a method which explicitly accounts for microstructure by modelling disorder quasirandomly on a supercell.

3.3.1 A short note on the cluster formulation

The SQS method is based on the cluster expansion formalism, and hence a brief introduction to this formalism will be given first. The essential idea is to identify the different "clusters" or "figures" making up the crystal structure, where each cluster consists of a subset of atoms in the crystal. The crystal is then described in terms of the different clusters. Conceptually this is similar to expressing a complicated wavefunction as a sum of simpler basis functions, where the crystal is the analogue of the wavefunction, and the clusters that of the basis functions.

Each lattice site i is assigned a "spin variable" σ_i, which can signify spin or, as is the case here, an atomic species. Depending on the number of alloyed species M, σ_i may take different values. E.g. for $M = 2$, $\sigma_i = \pm 1$ and for $M = 3$, $\sigma_i = \pm 1, 0$. Then the full lattice is described in terms of its clusters $f_p(k, m)$, where k denotes how many lattice sites are part of the cluster, m denotes the nearest neighbour shell or order, and p the position and orientation of the cluster f. Examples of clusters can be seen in figure 3.3.1(a), where three two-site ($k = 2$) clusters and one three-site ($k = 3$) cluster are depicted. Out of the three two-site clusters, $f_p(2, 1)$, $f_q(2, 1)$ and $f(2, 2)$, the first two are first order clusters ($m = 1$) with different position and orientation indicated by the subscripts p and q, and for the ordered solid shown in figure 3.3.1(a) they are symmetrically equivalent. The latter, $f(2, 2)$, is a second order ($m = 2$) cluster. The different orders are indicated in figure 3.3.1(b). The three-site cluster in figure 3.3.1(a) is of first order, since it is the smallest possible three-site cluster and can be found within the first next neighbour shell from the blue coloured atom. For clusters larger than two-sites, the chosen notation with m specifying the order is ambiguous without further definitions of how m is to be interpreted. However, since this section only aims to give a qualitative understanding of the topic of cluster expansion it is enough knowing that clusters involving different number of lattice sites and of different orders can be identified within any crystal, without going into further detail on how to label them.

The next step in the procedure is to define a set of M orthogonal polynomials $\Theta_n(\sigma_i)$ for each lattice site i. The index n runs between 0 and $M-1$. Hence for the simplest case of $M = 2$, as in figure 3.3.1(a), there are only two such polynomials per lattice site, which are found to be $\Theta_0(\sigma_i) = 1$ and $\Theta_1(\sigma_i) = \sigma_i$. How they are constructed can be found in ref. 87.

Finally the cluster characteristic functions $\Phi_f^n(\boldsymbol{\sigma})$ are defined as:

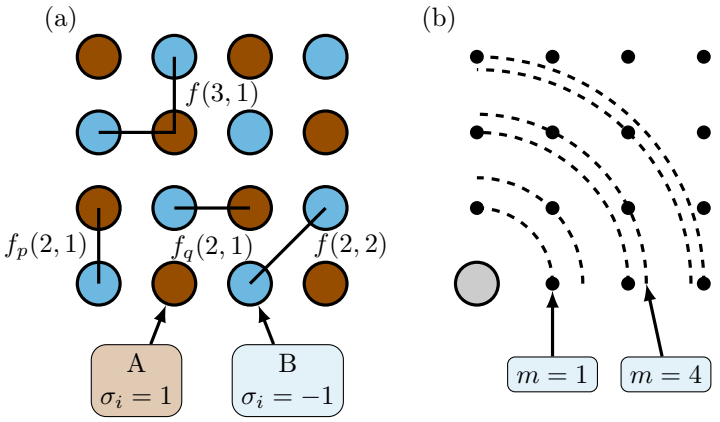

Figure 3.3.1: *(a) shows four clusters $f(k, m)$ of different order m and numbers of sites k. The clusters f_p and f_q are symmetrically equivalent. The two different species A and B are implied by brown and blue respectively. (b) shows the closest neighbour shells to the larger grey site in the bottom left corner, indicating clusters of different order.*

$$\Phi_f^n(\boldsymbol{\sigma}) = \prod_{i \in f} \Theta_n(\sigma_i). \tag{3.16}$$

For a specific lattice and concentration of atomic species, a lattice average $\bar{\Phi}_f(\boldsymbol{\sigma})$ can be found for each characteristic function. This can be used to describe any crystal in terms of its clusters, and for attaining the energy or other expectation values of the structure. This is not something that will be further discussed here, but more details can again be found in ref. 87. What is important to this discussion is that they can be used to describe disorder in a solid, which is utilised in the SQS method described below.

3.3.2 Special quasirandom structures

When considering disorder there are two different approaches: either the effect of disorder is considered explicitly, or on average. To accurately model the electronic effects of disorder in a material, it is often not enough to purely consider average effects, but disorder must be considered explicitly. This can be done by constructing a supercell with the alloyed elements randomly assigned to the lattice sites, relax the ionic positions of the supercell and find the electronic ground state. The primary problem with this approach is that the computational cost increases drastically with the number of atoms, i.e. large supercells are computationally expensive to model.

Due to an artificial periodicity introduced by the periodic boundary conditions, it is important to converge any supercell computation with respect to supercell size, and in addition it is not immediately obvious whether any particular (pseudo) random population of lattice sites provides a good representation of the true random alloy.

There isn't all that much to be done about the requirement to converge computations with respect to supercell size without reverting to methods only considering average effects of disorder, but the problem of accurately representing the random alloy on the supercell can indeed by amended to some extent through the generation of special quasi random structures (SQS),[86] rather than (pseudo) random ones. The idea is to, given a supercell size, find the configuration that best mimics the site population of the true random alloy. The best structure is chosen by considering the $\bar{\Phi}_f(\boldsymbol{\sigma})$ of clusters in the supercell, and trying to match those to the values for the true random alloy. In practise the alloy is most commonly assumed to be completely random, but this is not a fundamental assumption of the method. The SQS is found through construction of supercells according to specified alloying species and concentrations, evaluating the $\bar{\Phi}_f(\boldsymbol{\sigma})$, called correlation functions in this context, and comparing them to those of the true random alloy. The better they agree, the better the SQS mimics the true random alloy.

Since the supercell on which the SQS is constructed is of finite size, only clusters up to a certain order are meaningful to include, and therefore there are limitations on how small supercells can be and still give meaningful results. Therefore one should in principle always confirm convergence of the relevant physical aspects with respect to supercell size, although this might not always be feasible due to computational limitations.

Chapter 4

Modelling of chemical bonding in solids

Bonding is a widespread and commonly pondered upon topic within chemistry, and it is a way to describe interaction between atoms in various compounds. For a diatomic molecule, it is quite intuitive to identify the bond strength through the energy needed to break the single bond in that molecule or the force induced by stretching the bond, but for larger molecules it is not as trivial since all atoms interact with each other, and it is rarely possible to view the separation of the molecule into two parts as only breaking a single bond. The same problem carries over to crystals, which in a sense are just extended molecules. At the same time, different interactions within a molecule or crystal can clearly exhibit different characteristics, for example manifested through anisotropy in solid state phases. Hence it would clearly be interesting to have some way to estimate or rate the interaction between atoms in different compounds, which is exactly what will be considered in this chapter.

First, the Bader partitioning scheme is presented, which is a method for assigning charge to charge maxima, indicating charge transfer between atoms and thus serving as a measure of the ionic bonding characteristics. Next the crystal orbital Hamilton population (COHP) is considered, which gives an indication on covalency, and finally a bond projection of the force constants, which were introduced in chapter 3.1, is considered.

4.1 Bader analysis

Bader partitioning is a scheme used to estimate ionic bonding in a molecule or crystal, by assigning charge to identified charge maxima. There are

several different schemes for this purpose, where the Bader scheme has the advantage of being independent on the basis functions used for the charge density representation. The key idea is to identify charge maxima in the atomic structure as separated by dividing surfaces defined by the density gradient being zero along the surface normal. The charge assigned to each maximum is then attained by integrating over the charge distribution within the volume defined by the dividing surfaces.

One way of performing the Bader partitioning is by expressing the charge density on a regular grid, and assign each grid point to a charge maximum by following the density gradient.[88] These maxima commonly correlate with the ionic positions, but they need not do so and are not assumed to do so from the design of the algorithm. The charge assigned to each maximum is found by summing over all grid points assigned to said maximum. This straightforward way, not utilising any advanced interpolation scheme or explicitly finding the dividing surfaces, requires a grid dense enough for linear interpolation between the grid points to be sufficient. The computational efforts required scales linearly with the number of grid points, and in the initial proposal of this algorithm it was found that the convergence with respect to grid point density was similar to that of more computationally demanding schemes depending on more advanced interpolation.[88]

The grid based Bader partitioning has the additional advantages of being easy to implement, computationally efficient, and robust compared to earlier proposed schemes. Later papers has amended a shortcoming in the original algorithm proposed by Henkelman et. al.,[88] which fails to fully converge the Bader volumes with respect to increasing grid density by incorrectly assigning grid points to maxima in a way that favours dividing surfaces following the direction of the grid.[89–91]

4.2 Crystal orbital Hamilton population

A crystal orbital Hamilton population (COHP) is an energy weighted overlap integral between two quantum states. The concept is specifically designed to quantify bonds within solid state structures, and aims to give a qualitative estimate of the covalent characteristics of a bond. To define the COHP, we start by defining one electron wavefunctions $|\psi_j\rangle$ as linear combinations of atomic wave functions $|\chi_\mu\rangle$:

$$|\psi_j\rangle = \sum_\mu c_{\mu j} |\chi_\mu\rangle \,. \tag{4.1}$$

Here j stands for band index, and μ is shorthand notation for a specific orbital denoted by angular momentum l and quantum number m_l at lattice

site R within the unit cell. The $c_{\mu j}$ are the mixing coefficients $\langle\chi_\mu|\psi_j\rangle$. The overlap matrix $S_{\mu\nu}$ is defined as

$$S_{\mu\nu} = \langle\chi_\mu|\chi_\nu\rangle\,, \tag{4.2}$$

and because of the orthogonality of the wave function, we also have that

$$\begin{aligned}\delta_{ij} = \langle\psi_j|\psi_i\rangle &= \sum_\mu\sum_\nu \langle\psi_j|\chi_\mu\rangle\,\langle\chi_\mu|\chi_\nu\rangle\,\langle\chi_\nu|\psi_i\rangle \\ &= \sum_\mu\sum_\nu c^*_{\mu j} S_{\mu\nu} c_{\nu i}.\end{aligned} \tag{4.3}$$

The one-particle Schrödinger equation for the state $|\psi_j\rangle$ can be written as

$$\begin{aligned}(\hat{H}-\epsilon_j)\,|\psi_j\rangle = 0 &\Rightarrow \langle\chi_\mu|\,(\hat{H}-\epsilon_j)\sum_\nu c_{\nu j}\,|\chi_\nu\rangle = 0 \\ &\Rightarrow \sum_\nu c_{\nu j}\,\langle\chi_\mu|\,(\hat{H}-\epsilon_j)\,|\chi_\nu\rangle = 0 \\ &\Rightarrow \sum_\nu c_{\nu j}(\langle\chi_\mu|\,\hat{H}\,|\chi_\nu\rangle - \epsilon_j S_{\mu\nu}) = \sum_\nu (H_{\mu\nu}-\epsilon_j S_{\mu\nu})c_{\nu j} = 0.\end{aligned}$$

Multiplying by $c^*_{\mu i}$ from the left, summing over μ and using equation (4.3) yields

$$\begin{aligned}&\sum_\mu\sum_\nu c^*_{\mu i}(H_{\mu\nu}-\epsilon_j S_{\mu\nu})c_{\nu j} = 0 \\ \Rightarrow &\sum_\mu\sum_\nu c^*_{\mu i}H_{\mu\nu}c_{\nu j} = \sum_\mu\sum_\nu c^*_{\mu i}\epsilon_j S_{\mu\nu}c_{\nu j} = \epsilon_j\,\langle\psi_i|\psi_j\rangle = \epsilon_j\delta_{ij},\end{aligned} \tag{4.4}$$

so that we now have an expression for the one electron energies ϵ_j. We then express the so called band structure energy E_{band} as the energy integral over one electron occupation numbers f_j, and substitute for the band energy ϵ_j:

$$
\begin{aligned}
E_{band} &= \int^{\epsilon_F} d\epsilon \sum_j f_j \epsilon_j \delta(\epsilon_j - \epsilon) \\
&= \int^{\epsilon_F} d\epsilon \sum_j f_j \sum_\mu \sum_\nu c^*_{\mu j} H_{\mu\nu} c_{\nu j} \delta(\epsilon_j - \epsilon) \\
&= \int^{\epsilon_F} d\epsilon \sum_\mu \sum_\nu H_{\mu\nu} \underbrace{\sum_j f_j c^*_{\mu j} c_{\nu j} \delta(\epsilon_j - \epsilon)}_{\text{DOS matrix}} \\
&= \int^{\epsilon_F} d\epsilon \sum_\mu \sum_\nu H_{\mu\nu} N_{\mu\nu}(\epsilon) \\
&= \int^{\epsilon_F} d\epsilon \sum_\mu \sum_\nu COHP_{\mu\nu}(\epsilon). \qquad (4.5)
\end{aligned}
$$

Equation (4.5) defines the COHP, which is the contribution to the total band structure energy from the atomic orbitals μ and ν. The COHP has two contributions, the Hamiltonian matrix element $H_{\mu\nu} = \langle \chi_\mu | \hat{H} | \chi_\nu \rangle$, which can be positive, zero or negative, and the DOS-matrix element $N_{\mu\nu}$, which is strictly positive or zero. Thus the COHP is a function of energy, and can be positive, negative, or zero.

Equation (4.5) can be divided into two contributions: on-site COHPs ($R = R'$), corresponding to atomic contributions, and off-site contributions ($R \neq R'$). The latter can be interpreted as bonding descriptors of the interaction between two states μ and ν, and represent the covalent contribution of the bond [92]. By performing the energy integral, the so-called integrated COHP (iCOHP) is obtained, which is related to the energy of the bond between the two involved states. A thorough discussion on the correspondence between the iCOHP and bond energy can be found in the original work, [92] with the main conclusion that although the iCOHP in general can not be used as a quantitative measure of the bond energy, it is nevertheless a sensible descriptor for qualitative bond characteristics. Commonly, the COHPs from all possible combinations of μ and ν at the two sites R and R' are then summed to yield a total COHP for the two sites, which describes the overall characteristics of the particular bond.

4.2.1 COHP with a plane wave basis set

The theoretical derivation of the COHP presented in the previous section makes it clear that the very concept of COHP is highly local in nature, since it describes the electronic structure in terms of atomically centred wave

functions χ_μ. At the same time, some of the most popular and versatile electronic structure codes use a plane-wave basis set, as is the case for the VASP code used exclusively in this work. The band functions ψ_j are then in addition to the position $\mathbf{r}$ also functions of the wave vector $\mathbf{k}$. We may, however, carry through with an analogous procedure as previously, but the wavefunctions ψ_j now also carry a $\mathbf{k}$-dependence. This procedure is outlined in detail in reference 93, and results in a so called projected COHP (pCOHP) which carries a $\mathbf{k}$-dependence. Performing an integration over $\mathbf{k}$ results in the real-space pCOHP, which for a few selected structures is shown to be qualitatively very similar to the COHP attained from an electron structure computation based on a local basis set.[93]

Another complication arising in performing COHP analysis on results from a plane-wave basis code comes from the use of the PAW method, outlined in chapter 2.3. Fortunately enough, there is a work-around to this problem too 94, through the development of a projection scheme for the PAW method augmentation wavefunctions. This needs some generalisations compared to the previously presented scheme, related to the augmentation wavefunctions not being necessarily orthogonal. The generalised projection scheme is shown to produce results which compare well with those produced using a local basis set for both covalent and metallic solids. It is also shown to give a better projected DOS than the built in method of VASP, which is why it is used to evaluate the DOS throughout the work of this thesis.

4.2.2 The difference between COHP and DOS

We end this part of the chapter with a small example, demonstrating the difference between the DOS and (p)COHP. Figure 4.2.1 shows the partial and total DOS in panel a), and the total $-$pCOHP and partial $-$pCOHP for a specific bond in b), for the layered MAB phase Ti_4MoSiB_2 studied in Paper I. The 12 shortest bonds are considered for the evaluation of the total $-$pCOHP, which was found sufficient for convergence. Due to convention, the $-$pCOHP is shown rather than the pCOHP, coming from a wish to maintain analogy with an earlier bonding descriptor called crystal orbital overlap population (COOP), since positive COOP corresponds to bonding regions and negative to antibonding[95].

For the DOS, shown in panel a), we see that there are plenty of available states above the Fermi level, primarily coming from the Ti-atoms. However, looking at the total $-$pCOHP shown in panel b) by dark green, there are only a small contribution from bonding states (positive $-$pCOHP), indicating that although there are plenty of available states at the Fermi level, there are not that many states available that would actually lower the total energy if populated. Thus, the Ti_4MoSiB_2 structure is rather well

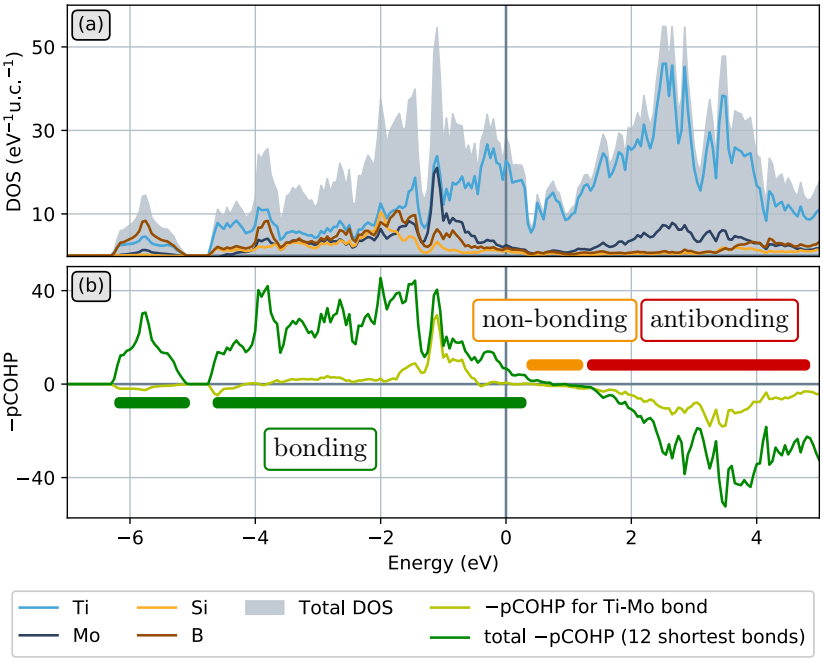

Figure 4.2.1: *DOS and −pCOHP for the quaternary boride Ti_4MoSiB_2 investigated in Paper I. The Fermi level is set at zero energy along the x-axis. (a) DOS and partial DOS of the four different species: Ti, Mo, Si and B. (b) −pCOHP summed over all orbitals for the Ti-Mo interaction in bright green, and the total −pCOHP in darker green. Green, yellow and red bars indicate bonding, non-bonding and antibonding regions of the total −pCOHP respectively.*

optimised from a bonding perspective, with the Fermi level being close to the region of non-bonding states (zero −pCOHP). Optimally, all bonding states should be filled, while all antibonding states (negative −pCOHP) should be empty. The green, yellow and red bars indicate the bonding, non-bonding and antibonding regions of the −pCOHP, respectively

Another thing to note is the peak in the Ti and Mo partial DOS at −1 eV below the Fermi level. In the −pCOHP corresponding to the Ti-Mo bond, shown in light green in panel b), we see that this peak corresponds to considerable bonding contributions to the −pCOHP coming from the Ti-Mo interaction. We can also see that besides this peak, the Ti-Mo interaction does not contribute significantly to the bonding of this material.

4.3 Force constants as bond descriptors

The last bonding descriptor to be discussed here is that of the force constants in a solid. The force constants correspond to the second order derivatives of the crystal potential energy with respect to lattice site displacements, as described in chapter 3.1, and thus they relate displacements of any two atoms to each other. The force constant between any two atoms is represented by a 3 by 3 matrix, and a few different ways of reducing them to a scalar value have been proposed in the literature, e.g. by taking the trace which is invariant with respect to coordinate rotations,[28,96] or by projecting the force constant along the vector between the two involved atoms[97]. Within the work presented in this thesis, the latter has been used.

Chapter 5

Summary and Outlook

Paper I

Investigation of Out-Of-Plane Ordered Ti_4MoSiB_2 from First Principles

Journal of Physics: Condensed Matter, 2022, **34**, 185501

In this project the bonding properties of the out-of-plane ordered quaternary boride Ti_4MoSiB_2 were compared to those of its ternary counterparts Ti_5SiB_2 and Mo_5SiB_2. Ti_4MoSiB_2 is a recently discovered compound,[84] which was theoretically predicted by the means described in chapter 3, and then successfully synthesised experimentally and converted into a 2D titanium oxide. Another 50 quaternary borides on this structure were predicted stable in the same study, out of which ten also display out-of-plane order, while the rest were predicted to display disorder.

All the structures considered in ref. 84 belong to the family of structures called T2 phases. Binary T2 phases were investigated during the 1950's[17,98], and the ternary Mo_5SiB_2 was first reported in 1957,[16] where B and Si were assumed in solid solution, with the detailed crystal structure established soon after.[17] However, Ti_5SiB_2 has to the best of our knowledge never been reported and is also predicted unstable in ref. 84. Yet, Ti_4MoSiB_2 is stable, a curiosity this project aims to understand. Additionally, the mechanical properties of the three phases are investigated from first principles.

Bonding analysis was carried out using the three methods described in chapter 4. The discussion included the 12 shortest bonds, with main focus on the 6 shortest of these, which were found to be the most important from the COHP analysis. The characteristics of five of these bonds didn't show

distinct differences between the three structures, whereas the bond between the two different metallic sites showed a distinct peak of bonding states close to the Fermi level, shown in Figure 4.2.1 for Ti_4MoSiB_2. For the two stable phases this bonding peak was found to be completely filled, while for Ti_5SiB_2 it is partially empty. The instability of Ti_5SiB_2 was thus suggested to be due to this peak of bonding states not being completely populated, rendering Ti_5SiB_2 energetically disfavoured to other Ti-containing phases.

Paper II

Investigation of 2D Boridene from First Principles and Experiments

Advanced Functional Materials, 2022, **32**, 2109060

In this project the properties of the novel 2D boridene $Mo_{4/3}B_2T_z$, first reported in ref. 36, were investigated both computationally and experimentally. Boridene is etched from the hexagonal *i*-MAB phase $(Mo_{2/3}Y_{1/3})_2AlB_2$ where the Mo and Y species populate the transition metal layer with in-plane order[99]. Upon etching of the parent phase $(Mo_{2/3}Y_{1/3})_2AlB_2$, Al and Y are removed, leaving the boridene $Mo_{4/3}B_2T_z$ which thus has vacancies where the minority transition metal element, Y in this case, used to sit in the parent MAB phase. In-plane ordered vacancies originating from the in-plane order of the parent phase are also observed for etching of *i*-MAX phases[100].

The project is focused on investigation of the terminations of boridene, from both computational and experimental perspectives, with a detailed XPS analysis performed to determine the concentrations of different terminating species. Just as for MXenes prepared by similar methods as the boridene, terminations were found to consist of a mixture of O, F and OH species. Computational analysis of termination sites and band structure for different terminations was then performed, showing that for termination with only a single species, the boridene is likely to be a small bandgap semiconductor. However, with terminations of mixed species, as determined through the XPS analysis, metallic behaviour was found to be more likely. An optical absorption measurement of the boridene showed no peaks in the visible to UV-range, indeed implying a metallic behaviour.

The dynamical stability was assessed through evaluation of the phonon dispersion for all structures with ordered terminations, as described in chapter 3.1. Stable structures were identified for all considered terminations, while the unterminated or bare boridene was found to be dynamically unstable. For structures with disordered terminations, the dynamical stability was not considered because of the considerable computational efforts

needed, making the procedure unfeasible. Finally, the boridene was considered for the hydrogen evolution reaction (HER), and was found to display promising properties with high activity and a low onset potential which further decreased during the experiment, a behaviour which has been seen also in *i*-MXenes.[101]

Paper III

Computational Screening of Chalcogen-Terminated Multilayer MXenes and M_2AX Precursors

Submitted

This study addresses the transition metal carbochalcogenides (TMCCs), which are a family of vdW bonded solids with the general formula M_2CCh_2, where M is a transition metal element, C is carbon and Ch is a chalcogen element. The individual layers of a TMCC have the structure of chalcogen terminated MXene sheets, which can be seen in Figure 1.1.1c), where the TMCC structures is shown schematically. In a recent study the two TMCCs Nb_2CS_2 and Ta_2CS_2 were exfoliated into single sheet MXene (ss-MXene) by intercalation, sparking new interest in the TMCCs, or multilayer (ml-)MXenes, as we have chosen to call them to highlight their structural characteristics[102].

The possibility for realisation of additional ss-MXene through exfoliation of ml-MXene phases is therefore considered here, by evaluation of the thermodynamical and dynamical stability of additional hypothetical ml-MXenes and successive assessment of the possibility for delamination, via the interlayer binding energy. M_2CCh_2 are considered with M=Sc, Y, Ti, Zr, Hf, V, Nb, Ta, Mo and W, and Ch=S, Se and Te. Seven thermodynamically and dynamically stable ml-MXenes are identified, where V_2CSe_2 incorporates a new transition metal compared to previously reported phases. Additionally, we consider the family of MAX phases for the indicated compositions, because the synthesis route for Nb_2CS_2 is based on manipulation of the corresponding MAX phase[103]. We identify 15 thermodynamically stable MAX phases. All the identified stable ml-MXenes are found to have similar binding energies, indicating that they should all be possible to exfoliate into the corresponding MXene.

Further, the electronic properties of the ml- and ss-MXenes are assessed by calculation of the band structure and density of states for each structure. Depending on the exact configuration of the chalcogen terminations, the materials may be conductors, small-bandgap semiconductors or semimetals. Exfoliation into 2D affects the electronic structure moderately, with the ml-MXenes that are predicted to be zero-bandgap semiconductors or

semimetals generally becoming finite bandgap semiconductors upon exfoliation, due to a systematic separation of the electronic bands upon exfoliation.

Paper IV

Computational Screening of the MOX_2 Transition Metal Oxydihalides with M=V, Nb, Ta, Mo, Ru and Os, and X=Cl, Br, I

In manuscript

This project studies the family of transition metal oxyhalides MOX_2. These are van der Waals (vdW) bonded layered materials, consisting of oxygen-transition metal chains bound together by O-atoms into a rectangular lattice, and decorated by halogens on each side. Two of the MOX_2 family members have been reported in single layer form, $NbOCl_2$ and $NbOI_2$ [9,25], both of which show intriguing optical properties. In this work, the electronic properties of all members of this family are studied. A number of phases not reported experimentally are also included, to cover all possible compositions given the elements which have been experimentally found in these phases, i.e. M=V, Nb, Ta, Mo, Ru and Os, and X=Cl, Br and I. The thermodynamical stability of all phases is assessed by comparison to the Materials Project database, as is the dynamical stability by evaluation of the phonon dispersion.

The bulk phase of all but one of the considered compositions is predicted to be thermodynamically stable, and all are found to be dynamically stable in both bulk and 2D forms. Four different prototype structures are identified for the family, with different types of distortions introduced to the most symmetrical prototype. Firstly, there is an in-plane Peierls distortion along the direction of the M-M bonds, causing the M-atoms to form localised dimers. This behaviour indicates a pseudo-1D nature of the transition metal chains. This distortion is observed for MOX_2 with M=V, Nb, Ta or Mo. For M=V and Nb, an additional distortion along the perpendicular in-plane direction of the M-O bonds is observed. This is referred to as a pseudo Jahn-Teller (pJT) distortion and causes these materials to be ferroelectric. For M=V, previous computational studies suggest magnetically ordered ground states without Peierls distortions [7,104], with results in the last prototype which only have the pJT distortions.

The most symmetrical phases which exhibit no Peierls distortion, $RuOX_2$ and $OsOX_2$, has a band structure which shows conducting behaviour. Upon introducing the Peierls distortion, a bandgap opens up for the VOX_2, $NbOX_2$ and $TaOX_2$ structures. There is a highly localised populated state

in the gap, originating from the dimerisation of the transition metal atoms. Optical transition directly from the localized state to the conduction band minima (cbm) is forbidden since both are primarily contributed to by transition metal d-states. Therefore, the gap between the cbm and valence band maxima (vbm) disregarding the localised dimer state was considered for analysis of bandgap trends, since the vbm constitutes of halogen p-states. We observe that this extended bandgap is primarily related to the halogen size, and it decreases with increasing size of the halogen. We further identify the set of Ta-based phases, $TaOX_2$, as being most similar to the set of $NbOX_2$ phases. In particular, the dimerisation in terms of dimer bond length relative to transition metal covalent radius in $TaOI_2$ is slightly stronger than in $NbOI_2$ which suggest that $TaOI_2$ could display nonlinear optical effects similar in strength as seen in $NbOI_2$ [105].

Paper V

Expanding the Structural and Compositional Space of 2D $M_2X_2T_y$ Materials through Simulated Etching of 3D YM_2X_2 Parent Phases

In manuscript

This project is a follow-up study of a screening study where a 2D material, $Ru_2Si_xO_y$, was predicted and successively synthesised. This is exciting from two perspectives. Firstly, $Ru_2Si_xO_y$ was predicted using a newly developed methodology for predicting chemically exfoliated materials. This methodology is the first computational framework to successfully explain the etching (and lack of etching) of MAX-phases into MXene, which has long been a challenge to the community of computational 2D materials. Secondly, it is exciting because $Ru_2Si_xO_y$ belongs to a completely new family of 2D materials, and is etched from parent phase belonging to a very large family of layered 3D phases with formula AM_2X_2.

The study consists of three steps. Firstly, a large compositional space is screened for thermodynamical stability of potential parent phases AM_2X_2. We consider A=Y, which is the element that is expected to be removed in the etching process, specifically because $Ru_2Si_xO_y$ was synthesised by removal of Y from the parent phase YRu_2Si_2. For the M-site, all 3d, 4d and 5d transition metal elements were considered, except Sc and Y (because they are found at the A-site of the YM_2X_2 materials), and Cd and Hg (because of their high toxicity). For the X-site, the elements Al, Ga, In, Si, Ge, Sn, P, As, Sb, S, Se, and Te were considered. Out of these 300 compounds, 31 were predicted as thermodynamically stable, and another 6 as close enough to being thermodynamically stable that they were included in

the next step of analysis. Thus, 37 potential 3D structures were identified, out of which nine are not experimentally reported.

In the second step, the newly developed methodology is employed to simulate the etching process for the 37 potential parent phases identified in the first step[106,107]. This was done by considering the possibility for vacancy formation of the different constituent elements, requiring that it should be thermodynamically preferable to form a Y-vacancy while not to form an M- or X-vacancy. This procedure identified 24 of the 37 proposed parent phases as promising. Additionally, the potential for chemical etching was assessed through the exfoliation and solvation free energies, requiring a phase to prefer exoliation to no etching and to complete solvation. 17 out of the 24 promising phases also proved favourable from this perspective, which identifies them as possible to etch chemically and predicts a corresponding 2D material for each 3D phase.

In the last step, the dynamical stability of the predicted 2D materials were assessed, and their electronic properties were simulated through calculation of band structure and density of states (DOS). 15 out of the 17 2D materials predicted in the second step were deemed dynamically stable. Nine of the 15 predicted 2D structures are reported here for the first time, and three of those are etched from parent phases not previously assessed through the simulated etching methodology. The electronic property simulations indicate metallic behaviour for most 2D materials, while four show semimetallic properties.

Contribution to the Field

The work concluded within the scope of this thesis can be said to be either sprawling or broad, depending on ones attitude. It does not claim to cover significant ground within any specific subfield of two dimensional materials science, but instead it makes a dent on several different places on the border to that subset of human knowledge. The work within this thesis considers both 3D and 2D materials, with Paper I, which only considers a 3D structure, and II, which focus solely on a derived 2D material, each being the extreme on this scale. For the remaining three manuscripts, a more complete view has been adopted, where each project starts from a layered 3D material and ends with the corresponding 2D derivative. These three manuscripts are also more complete from the perspective that they are all screening studies, covering not only one or a small set of structures, but instead address a larger compositional space. Simultaneously, they might be deemed less complete as well, from the perspective that they are purely computational.

This thesis adds to our understanding of bonding characteristics in the set of laminated borides $M_4M'SiB_2$, and it contributes insights into the

termination concentration of boridene, the first 2D boride, and its effect on the electronic properties of this material. It also predicts expansions to two well established families of vdW structures, and summarises and puts into some perspective previous literature on these respective families. And finally, it pokes at truly the forefront of development in the field of 2D materials, by exploring the entire process of selective etching, from the identification of potential parent phases all the way to the prediction of novel 2D materials.

Outlook

So again comes the question: where do we go from here? The herein presented computational work claims multiple predictions and suggest several possible implications, but all computational conclusions ultimately need experimental verification; Where *do* the chalcogen-terminations sit on ml-MXene? What *are* their electronic properties? Are the VOX_2 structures magnetic or do they dimerise? Do $TaOX_2$ exhibit second harmonic generation? Can we actually etch YM_2X_2 into the respective predicted 2D materials? And so on. However, given the experimental insights required to answer any of these questions, one might say they are outside the scope of an outlook accompanying a work as computationally focused as the present one.

Conforming to the computational nature of this thesis, there are alternative directions to pursue. The already established 2D structures discussed in this thesis could be studied in more detail, in particular those that we predict, but also those which are already realised. By introducing distortions corresponding to the imaginary branches of the YM_2X_2 derivatives found to be dynamically unstable, perhaps even more different 2D structures could be identified as derivatives of the YM_2X_2 materials. Additionally, there are suggested expansions to the MOX_2 family which are computationally shown to exhibit curious properties, for which a thermodynamical stability analysis is lacking but highly motivated[108,109]. There are also a number of large scale screening studies predicting plenty of 2D materials[5,107], as well as materials databases dedicated to 2D phases[110], where candidate 2D materials and structures for further study may be found.

Remaining closer to the computational screening focus of the present work, perhaps the most obvious path forward would be to wield the methodology of simulated etching at yet more laminated materials. The family of $ThCr_2Si_2$ structures is far from depleted, and other families of chemically bound laminates exist as well. Additionally, other etching chemistries than that of HF acid could be considered, which may lead to predictions of additional 2D materials also in the systems already studied. There is really no end to the possibilities, which is in itself a central challenge within the

topic of materials design. It leads to an overwhelming parameter space, and although computational probing is vastly more efficient than experimental probing, computational screening is still a resource intense activity in terms of computation time. The natural next step in the development would be to include some machine learning aspect in the screening process, both to more effectively identify potential parent phases and to assess the possibility for exfoliation.

Thus, there is not a shortage of directions to consider in the search for the next generation of materials, but rather, as well put by Gandalf: All we have to decide is what to do with the time that is given us.

Bibliography

1. P. Siffert and E. F. Krimmel, *Silicon: Evolution and Future of a Technology*, 2004.

2. K. S. Novoselov, A. K. Geim, S. V. Morozov, D. Jiang, Y. Zhang, S. V. Dubonos, I. V. Grigorieva and A. A. Firsov, *Science*, 2004, **306**, 666–669.

3. M. Naguib, M. Kurtoglu, V. Presser, J. Lu, J. Niu, M. Heon, L. Hultman, Y. Gogotsi and M. W. Barsoum, *Advanced Materials*, 2011, **23**, 4248–4253.

4. H. Schäfer, E. Sibbing and R. Gerken, *Zeitschrift für anorganische und allgemeine Chemie*, 1961, **307**, 163–173.

5. N. Mounet, M. Gibertini, P. Schwaller, D. Campi, A. Merkys, A. Marrazzo, T. Sohier, I. E. Castelli, A. Cepellotti, G. Pizzi and N. Marzari, *Nature Nanotechnology*, 2018, **13**, 246–252.

6. H. Tan, M. Li, H. Liu, Z. Liu, Y. Li and W. Duan, *Physical Review B*, 2019, **99**, 195434.

7. H. Ai, X. Song, S. Qi, W. Li and M. Zhao, *Nanoscale*, 2019, **11**, 1103–1110.

8. Y. Jia, M. Zhao, G. Gou, X. C. Zeng and J. Li, *Nanoscale Horizons*, 2019, **4**, 1113–1123.

9. Q. Guo, X.-Z. Qi, L. Zhang, M. Gao, S. Hu, W. Zhou, W. Zang, X. Zhao, J. Wang, B. Yan, M. Xu, Y.-K. Wu, G. Eda, Z. Xiao, S. A. Yang, H. Gou, Y. Ping Feng, G.-C. Guo, W. Zhou, X.-F. Ren, C.-W. Qiu, S. J. Pennycook and A. T. S Wee, *Nature*, 2023, **613**, 53.

10. I. Abdelwahab, B. Tilmann, X. Zhao, I. Verzhbitskiy, R. Berté, G. Eda, W. L. Wilson, G. Grinblat, L. de S. Menezes, K. P. Loh and S. A. Maier, *Advanced Optical Materials*, 2023, **11**, 2202833.

11. M. Dahlqvist, M. W. Barsoum and J. Rosen, *Materials Today*, 2023.

12. H. Kudielka and H. Rohde, *Zeitschrift für Kristallographie*, 1960, **114**, 447–456.

13. O. Beckmann, H. Boller and H. Nowotny, *Monatshefte für Chemie*, 1970, **101**, 945–955.

14. M. W. Barsoum and T. El-Raghy, *Journal of the American Ceramic Society*, 1996, **79**, 1953–1956.

15. S. Kota, M. Sokol and M. W. Barsoum, *International Materials Reviews*, 2020, **65**, 226–255.

16. H. Nowotny, E. Dimakopoulou and H. Kudielka, *Monatshefte für Chemie und verwandte Teile anderer Wissenschaften*, 1957, **88**, 180–192.

17. B. Aronsson, *Acta Chemica Scandinavica*, 1958, **12**, 31–37.

18. Z. Ban and M. Sikirica, *Acta Crystallographica*, 1965, **18**, 594.

19. M. Shatruk, *Journal of Solid State Chemistry*, 2019, **272**, 198–209.

20. M. Chhowalla, H. S. Shin, G. Eda, L.-J. Li, K. P. Loh and H. Zhang, *Nature Chemistry*, 2013, **5**, 263–275.

21. D. Pacilé, J. C. Meyer, C. Ö. Girit and A. Zettl, *Applied Physics Letters*, 2008, **92**, 133107.

22. K. S. Novoselov, D. Jiang, F. Schedin, T. J. Booth, V. V. Khotkevich, S. V. Morozov and A. K. Geim, *Proceedings of the National Academy of Sciences*, 2005, **102**, 10451–10453.

23. L. D. Landau and E. M. Lifshitz, *Course of Theoretical Physics Vol. 5. Statistical Physics Part 1*, 1980, pp. 432–438.

24. J. Zhou, M. Dahlqvist, J. Björk and J. Rosen, *Chemical Reviews*, 2023, **123**, 13291–13322.

25. Y. Fang, F. Wang, R. Wang, T. Zhai and F. Huang, *Advanced Materials*, 2021, **33**, 2101505.

26. K. V. Mahesh, R. Rashada, M. Kiran, A. Peer Mohamed and S. Ananthakumar, *RSC Advances*, 2015, **5**, 51242–51247.

27. A. VahidMohammadi, J. Rosen and Y. Gogotsi, *Science*, 2021, **372**, eabf1581.

28. M. Khazaei, A. Ranjbar, K. Esfarjani, D. Bogdanovski, R. Dronskowski and S. Yunoki, *Physical Chemistry Chemical Physics*, 2018, **20**, 8579–8592.

29. H.-W. Wang, M. Naguib, K. Page, D. J. Wesolowski and Y. Gogotsi, *Chemistry of Materials*, 2016, **28**, 349–359.

30. M. Ghidiu, M. R. Lukatskaya, M.-Q. Zhao, Y. Gogotsi and M. W. Barsoum, *Nature*, 2014, **516**, 78–81.

31. J. Halim, M. R. Lukatskaya, K. M. Cook, J. Lu, C. R. Smith, L.-Å. Näslund, S. J. May, L. Hultman, Y. Gogotsi, P. Eklund and M. W. Barsoum, *Chemistry of Materials*, 2014, **26**, 2374–2381.

32. V. Natu, R. Pai, M. Sokol, M. Carey, V. Kalra and M. W. Barsoum, *Chem*, 2020, **6**, 616–630.

33. J. Lu, I. Persson, H. Lind, J. Palisaitis, M. Li, Y. Li, K. Chen, J. Zhou, S. Du, Z. Chai, Z. Huang, L. Hultman, P. Eklund, J. Rosen, Q. Huang and P. O. Å. Persson, *Nanoscale Advances*, 2019, **1**, 3680–3685.

34. V. Kamysbayev, A. S. Filatov, H. Hu, X. Rui, F. Lagunas, D. Wang, R. F. Klie and D. V. Talapin, *Science*, 2020, **369**, 979–983.

35. H. Lind, J. Halim, S. I. Simak and J. Rosen, *Physical Review Materials*, 2017, **1**, 44002.

36. J. Zhou, J. Palisaitis, J. Halim, M. Dahlqvist, Q. Tao, I. Persson, L. Hultman, P. O. Å. Persson and J. Rosen, *Science*, 2021, **373**, 801–805.

37. E. Schrödinger, *Physical Review*, 1926, **28**, 1049–1070.

38. M. Born and R. Oppenheimer, *Annalen der Physik*, 1927, **389**, 457–484.

39. L. H. Thomas, *Mathematical Proceedings of the Cambridge Philosophical Society*, 1927, **23**, 542 – 548.

40. E. Fermi, *Rend. Accad. Naz. Lincei*, 1927, **6**, 602–607.

41. E. Fermi, *Zeitschrift für Physik*, 1928, **48**, 73–79.

42. P. Hohenberg and W. Kohn, *Physical Review*, 1964, **136**, 864–871.

43. W. Kohn and L. J. Sham, *Physical Review*, 1965, **140**, 1133–1138.

44. K. Schönhammer, O. Gunnarsson and R. M. Noack, *Physical Review B*, 1995, **52**, 2504–2509.

45. K. Burke, J. Perdew and E. M., *Electron Density Functional Theory: Recent Progress and New Directions*, 1998, pp. 57–68.

46. A. D. Becke, *Journal of Chemical Physics*, 2014, **140**, 18A301.

47. D. M. Ceperley and B. J. Alder, *Physical Review Letters*, 1980, **45**, 566–569.

48. J. P. Perdew, K. Burke and M. Ernzerhof, *Physical Review Letters*, 1996, **77**, 3865–3868.

49. J. D. van der Waals, *PhD thesis*, 1873.

50. K. Berland, V. R. Cooper, K. Lee, E. Schröder, T. Thonhauser, P. Hyldgaard and B. I. Lundqvist, *Reports on Progress in Physics*, 2015, **78**, 066501.

51. H. Rydberg, N. Jacobson, P. Hyldgaard, S. I. Simak, B. I. Lundqvist and D. C. Langreth, *Surface Science*, 2003, **532-535**, 606–610.

52. M. Dion, H. Rydberg, E. Schröder, D. C. Langreth and B. I. Lundqvist, *Physical Review Letters*, 2004, **92**, 246401.

53. H. Rydberg, B. I. Lundqvist, D. C. Langreth and M. Dion, *Physical Review B*, 2000, **62**, 6997–7006.

54. H. Rydberg, M. Dion, N. Jacobson, E. Schröder, P. Hyldgaard, S. I. Simak, D. C. Langreth and B. I. Lundqvist, *Physical Review Letters*, 2003, **91**, 126402.

55. K. Lee, É. D. Murray, L. Kong, B. I. Lundqvist and D. C. Langreth, *Physical Review B*, 2010, **82**, 081101(R).

56. G. Román-Pérez and J. M. Soler, *Physical Review Letters*, 2009, **103**, 096102.

57. J. Klimes, D. R. Bowler and A. Michaelides, *Physical Review B*, 2011, **83**, 195131.

58. A. D. Becke, *The Journal of Chemical Physics*, 1986, **85**, 7184–7187.

59. J. P. Perdew, *International Journal of Quantum Chemistry*, 1985, **28**, 497–523.

60. A. D. Becke, *Journal of Chemical Physics*, 1993, **98**, 1372–1377.

61. A. D. Becke, *Journal of Chemical Physics*, 1993, **98**, 5648–5652.

62. J. P. Perdew, M. Ernzerhof and K. Burke, *Journal of Chemical Physics*, 1996, **105**, 9982–9985.

63. J. Heyd, G. E. Scuseria and M. Ernzerhof, *Journal of Chemical Physics*, 2003, **118**, 8207–8215.

64. J. Heyd, G. E. Scuseria and M. Ernzerhof, *Journal of Chemical Physics*, 2006, **124**, 219906.

65. J. Heyd and G. E. Scuseria, *Journal of Chemical Physics*, 2004, **121**, 1187–1192.

66. A. V. Krukau, O. A. Vydrov, A. F. Izmaylov and G. E. Scuseria, *Journal of Chemical Physics*, 2006, **125**, 224106.

67. M. Ernzerhof and G. E. Scuseria, *Journal of Chemical Physics*, 1999, **110**, 5029–5036.

68. C. Adamo and V. Barone, *Journal of Chemical Physics*, 1999, **110**, 6158–6170.

69. A. J. Garza and G. E. Scuseria, *Journal of Physical Chemistry Letters*, 2016, **7**, 4165–4170.

70. A. D. Becke and E. R. Johnson, *Journal of Chemical Physics*, 2006, **124**, 221101.

71. F. Tran and P. Blaha, *Physical Review Letters*, 2009, **102**, 226401.

72. R. T. Sharp and G. K. Horton, *Physical Review*, 1953, **90**, 317.

73. J. D. Talman and W. F. Shadwick, *Physical Review A*, 1976, **14**, 36–40.

74. P. Borlido, T. Aull, A. W. Huran, F. Tran, M. A. Marques and S. Botti, *Journal of Chemical Theory and Computation*, 2019, **15**, 5069–5079.

75. P. E. Blöchl, *Physical Review B*, 1994, **50**, 17953–17979.

76. H. Ibach and H. Lüth, *Solid-State Physics - An Introduction to Principles of Material Science*, Springer, 3rd edn, 2002.

77. G. Leibfried and W. Ludwig, *Solid State Physics Vol. 12*, 1961, p. 283.

78. F. Eriksson, E. Fransson and P. Erhart, *Advanced Theory and Simulations*, 2019, **2**, 1800184.

79. J. Carrete, W. Li, L. Lindsay, D. A. Broido, L. J. Gallego and N. Mingo, *Materials Research Letters*, 2016, **4**, 204–211.

80. M. Dahlqvist, B. Alling and J. Rosén, *Physical Review B*, 2010, **81**, 220102.

81. A. Carlsson, J. Rosen and M. Dahlqvist, *Physical Chemistry Chemical Physics*, 2022, **24**, 11249.

82. A. Thore, M. Dahlqvist, B. Alling and J. Rosén, *Computational Materials Science*, 2014, **91**, 251–257.

83. A. Poulou, T. A. Mellan and M. W. Finnis, *Physical Review Materials*, 2021, **5**, 033608.

84. M. Dahlqvist, J. Zhou, I. Persson, B. Ahmed, J. Lu, J. Halim, Q. Tao, J. Palisaitis, J. Thörnberg, P. Helmer, L. Hultman, P. O. Å. Persson and J. Rosen, *Advanced Materials*, 2021, **33**, 2008361.

85. Q. Tao, P. Helmer, L. Jouffret, M. Dahlqvist, J. Lu, J. Zhou and J. Rosen, *Crystal Growth and Design*, 2020, **20**, 7640–7646.

86. A. Zunger, S.-H. Wei, L. G. Ferreira and J. E. Bernard, *Physical Review Letters*, 1990, **65**, 353–356.

87. J. M. Sanchez, F. Ducastelle and D. Gratias, *Physica A: Statistical Mechanics and its Applications*, 1984, **128A**, 334–350.

88. G. Henkelman, A. Arnaldsson and H. Jónsson, *Computational Materials Science*, 2006, **36**, 354–360.

89. E. Sanville, S. D. Kenny, R. Smith and G. Henkelman, *Journal of Computational Chemistry*, 2007, **28**, 899–908.

90. W. Tang, E. Sanville and G. Henkelman, *Journal of Physics: Condensed Matter*, 2009, **21**, 084204.

91. M. Yu and D. R. Trinkle, *The Journal of Chemical Physics*, 2011, **134**, 064111.

92. R. Dronskowski and P. E. Blöchl, *The Journal of Chemical Physics*, 1993, **97**, 8617–8624.

93. V. L. Deringer, A. L. Tchougréeff and R. Dronskowski, *The Journal of Physical Chemistry A*, 2011, **115**, 5461–5466.

94. S. Maintz, V. L. Deringer, A. L. Tchougréeff and R. Dronskowski, *Journal of Computational Chemistry*, 2013, **34**, 2557–2567.

95. T. Hughbanks and R. Hoffmann, *Journal of American Chemical Society*, 1983, **105**, 3528–3537.

96. Y. Liu, K. T. Eddie Chua, T. C. Sum and C. K. Gan, *Physical Chemistry Chemical Physics*, 2014, **16**, 345–350.

97. V. L. Deringer, R. P. Stoffel, M. Wuttig and R. Dronskowski, *Chemical Science*, 2015, **6**, 5255–5262.

98. H. Nowotny, A. W. Searcy and J. E. Orr, *The Journal of Physical Chemistry*, 1956, **60**, 677.

99. M. Dahlqvist, Q. Tao, J. Zhou, J. Palisaitis, P. O. Å. Persson and J. Rosen, *Journal of the American Chemical Society*, 2020, **142**, 18583–18591.

100. Q. Tao, M. Dahlqvist, J. Lu, S. Kota, R. Meshkian, J. Halim, J. Palisaitis, L. Hultman, M. W. Barsoum, P. O. Å. Persson and J. Rosen, *Nature Communications*, 2017, **8**, 14949.

101. H. Lind, B. Wickman, J. Halim, G. Montserrat-Sisó, A. Hellman and J. Rosen, *Advanced Sustainable Systems*, 2021, **5**, 2000158.

102. A. Majed, M. Kothakonda, F. Wang, E. N. Tseng, K. Prenger, X. Zhang, P. O. Å. Persson, J. Wei, J. Sun and M. Naguib, *Advanced Materials*, 2022, **34**, 2200574.

103. H. Boller and K. Hiebl, *Journal of Alloys and Compounds*, 1992, **183**, 438–443.

104. A. Mahajan and S. Bhowmick, *Journal of Physical Chemistry C*, 2023, **127**, 11407–11418.

105. T. Fu, K. Bu, X. Sun, D. Wang, X. Feng, S. Guo, Z. Sun, Y. Fang, Q. Hu, Y. Ding, T. Zhai, F. Huang and X. Lü, *Journal of the American Chemical Society*, 2023, **145**, 16828–16834.

106. J. Björk, J. Halim, J. Zhou and J. Rosen, *npj 2D Materials and Applications*, 2023, **7**, 5.

107. J. Björk, J. Zhou, P. O. Å. Persson and J. Rosen, *accepted for publication in Science*, 2024, XX.

108. Q. Yang, D. Wang, Z. Y. Zeng, H. Y. Geng and X. R. Chen, *Physical Review B*, 2024, **109**, 035411.

109. M. Noor-A-Alam and M. Nolan, *Nanoscale*, 2022, **14**, 11676–11683.

110. J. Zhou, L. Shen, M. D. Costa, K. A. Persson, S. P. Ong, P. Huck, Y. Lu, X. Ma, Y. Chen, H. Tang and Y. P. Feng, *Scientific Data*, 2019, **6**, 1.

Papers

The papers associated with this thesis have been removed for copyright reasons. For more details about these see:

https://doi.org/10.3384/9789180755443

FACULTY OF SCIENCE AND ENGINEERING

Linköping Studies in Science and Technology, Dissertation No. 2376, 2024
Department of Physics, Chemistry and Biology

Linköping University
SE-581 83 Linköping, Sweden

www.liu.se

LINKÖPING UNIVERSITY